HHS Public Access

Author manuscript

Cell Rep. Author manuscript; available in PMC 2023 June 12.

Published in final edited form as:

Cell Rep. 2023 May 30; 42(5): 112429. doi:10.1016/j.celrep.2023.112429.

Cerebellar granule cell signaling is indispensable for normal motor performance

Joon-Hyuk Lee[1], **Mehak M. Khan**[1], **Amanda P. Stark**[1], **Soobin Seo**[1], **Aliya Norton**[1], **Zhiyi Yao**[1], **Christopher H. Chen**[1], **Wade G. Regehr**[1,2,*]

[1]Department of Neurobiology, Harvard Medical School, Boston, MA 02115, USA

[2]Lead contact

SUMMARY

Within the cerebellar cortex, mossy fibers (MFs) excite granule cells (GCs) that excite Purkinje cells (PCs), which provide outputs to the deep cerebellar nuclei (DCNs). It is well established that PC disruption produces motor deficits such as ataxia. This could arise from either decreases in ongoing PC-DCN inhibition, increases in the variability of PC firing, or disruption of the flow of MF-evoked signals. Remarkably, it is not known whether GCs are essential for normal motor function. Here we address this issue by selectively eliminating calcium channels that mediate transmission ($Ca_V2.1$, $Ca_V2.2$, and $Ca_V2.3$) in a combinatorial manner. We observe profound motor deficits but only when all Ca_V2 channels are eliminated. In these mice, the baseline rate and variability of PC firing are unaltered, and locomotion-dependent increases in PC firing are eliminated. We conclude that GCs are indispensable for normal motor performance and that disruption of MF-induced signals impairs motor performance.

Graphical abstract

*Correspondence: wade_regehr@hms.harvard.edu.

AUTHOR CONTRIBUTIONS

J.-H.L. and W.G.R. conceived the experiments. S.S., A.N., Z.Y., and J.-H.L. conducted behavioral experiments. J.-H.L. analyzed behavioral data. M.M.K. conducted electrophysiology experiments. J.-H.L. conducted virus injection experiments. A.P.S. and C.H.C. conducted *in vivo* recordings. J.-H.L. analyzed *in vivo* data. J.-H.L. plotted and visualized all figures. J.-H.L. and W.G.R. wrote the manuscript with input from the other authors.

DECLARATION OF INTERESTS

The authors declare no competing interests.

SUPPLEMENTAL INFORMATION

Supplemental information can be found online at https://doi.org/10.1016/j.celrep.2023.112429.

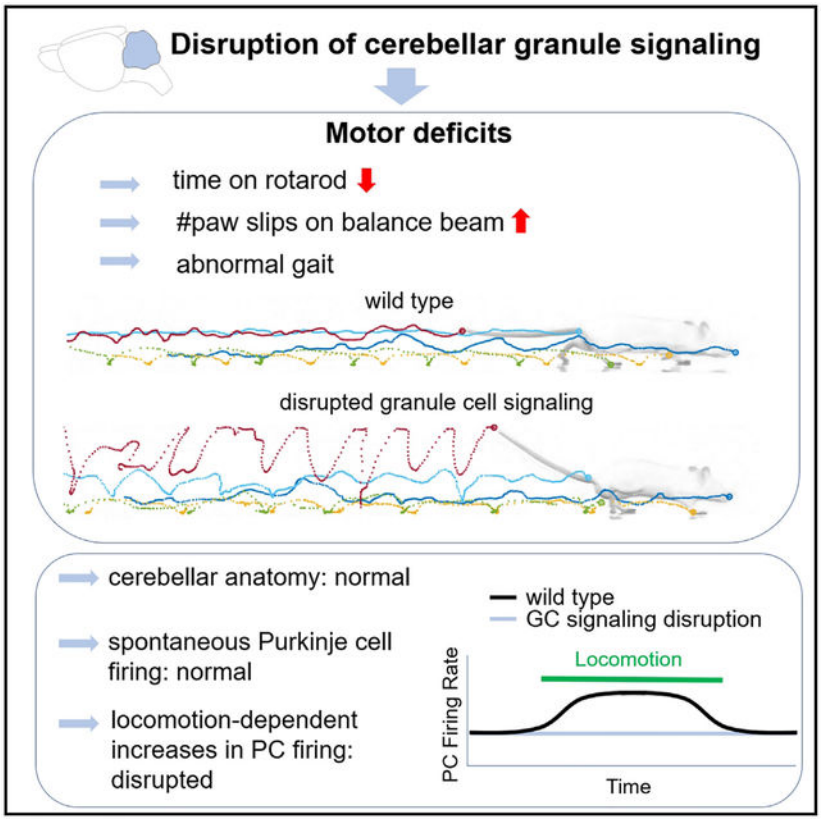

In brief

It is well established that the cerebellum is vital for normal motor performance, but whether granule cells are also essential is not known. Lee et al. show that disrupting granule cell signaling causes profound motor deficits, establishing that granule cells are crucial for normal motor performance.

INTRODUCTION

Deficits in the cerebellar cortex can impair motor performance and lead to deficits in gait and balance. The cerebellar cortex transforms mossy fiber (MF) inputs into granule cell (GC) activity patterns within the input layer, which, in turn, control the firing of Purkinje cells (PCs), the outputs of the cerebellar cortex[1] (Figure 1A). PCs inhibit cells in the deep cerebellar nuclei that convey cerebellar signals to the rest of the brain. PCs are spontaneously active and provide ongoing inhibition to deep nucleus neurons that have been implicated in ataxia.[2,3] Weakened PC signaling and PC death have been reported in motor deficits such as ataxia. This has been shown for selective expression in PCs of mutant ataxin-1[4] or mutant ataxin-2[5] and selective elimination from PCs of $Ca_V2.1$ calcium channels,[6] TSC1,[7] or MTSS1,[8] which suppress PC signaling and are accompanied by the death of many PCs.[4–7] It is not clear how disruption of PC signaling impairs motor performance, and several hypotheses have been advanced:[9–12] (1) disruption of MF-evoked

changes in PC firing and the influence they exert on deep nuclei, (2) preventing ongoing PC inhibition of deep nuclei, or (3) increasing the timing variability of PC firing.[12–20]

In contrast to the established importance of PCs to motor performance, the role of GCs remains unclear. Disruption of GC signaling is expected to prevent MF-evoked changes in PC firing, but it is unclear how it would influence spontaneous PC firing and ongoing inhibition of cerebellar nuclei. Selective suppression of synaptic transmission in GCs by cre-dependent doxycycline-activated expression of tetanus toxin did not lead to ataxia or tremor[21,22] but impaired performance on a fixed bar.[22] However, these results are difficult to interpret because GC transmission might not have been completely eliminated. Similarly, although $Ca_V2.1$ elimination from PCs leads to ataxia,[6] elimination of $Ca_V2.1$ from GCs does not.[23] This could be because GCs are not required for normal motor performance or because GC transmission was not completely eliminated. It has been proposed that GC signaling was not abolished in these mice because the most widely used cre-driver line to target GCs does not express cre in all GCs. In contrast, eliminating Munc18-1 in GCs led to mice that were unable to walk, but this manipulation was so severe that it was difficult to interpret.[24] The absence of GCs essentially eliminated the input layer, reduced the molecular layer thickness by 43%, and drastically altered PC morphology. The motor deficits in these mice could arise from these secondary effects.

Selective removal of all of the calcium channels that mediate synaptic transmission is a promising strategy to more completely eliminate GC signaling. However, this is complicated because $Ca_V2.1$, $Ca_V2.2$, and $Ca_V2.3$ calcium channels all contribute to glutamate release from GCs.[23,25,26] A recent study of calcium channels and synaptic transmission[27] suggested that genetically ablating $Ca_V2.1$, $Ca_V2.2$, and $Ca_V2.3$ could powerfully disrupt synaptic transmission to better assess the behavioral roles of GCs.

Here we determine whether cerebellar GCs are required for normal motor performance. We find that eliminating $Ca_V2.1$, $Ca_V2.2$, and $Ca_V2.3$ channels from GCs (GC triple knockout [TKO]) produces strong motor deficits. We find that, in GC TKO mice, synaptic transmission at GC-to-PC synapses is eliminated without disrupting the morphology of the cerebellar cortex. PCs fire spontaneously with similar frequencies and coefficients of variation in control and GC TKO mice, and running-induced increases in PC activity are only observed in control mice but not in GC TKO mice. These findings indicate that eliminating GC signaling impairs motor performance by disrupting MF-induced changes in PC firing rather than by altering the ongoing PC inhibition of deep cerebellar nucleus (DCN) neurons or by increasing the variability of PC firing.

RESULTS

The motor effects of graded elimination of Ca_V2 channels from GCs and PCs

To evaluate the relevance of GC signaling to motor performance, we generated mice in which we perturbed GC signaling by deleting Ca_V2s that evoke neurotransmitter release.[27] We also disrupted PC signaling in a similar manner to compare the effects of GC and PC manipulation. Previous studies eliminated $Ca_V2.1$ from PCs and observed ataxia,[6] whereas elimination of $Ca_V2.1$ from GCs did not impair motor performance.[23] We extended this

approach to evaluate the combinatorial elimination of Ca_V2s by using *floxed* alleles for conditional elimination of $Ca_V2.1$, $Ca_V2.2$, and $Ca_V2.3$[27–29] (Figure 1B; Table S1). We used PCP2-cre to target PCs[30,31] and GABRA6-cre and α6-cre to target GCs.[21,23,24,32–34] We generated mice expressing different combinations of Ca_V2s in targeted cells and then quantified the number of paw slips in a balance beam test for all littermates.[35] For GCs, deletion of either $Ca_V2.1$ alone or any two types of Ca_V2 channels did not increase the number of paw slips. We only observed motor deficits when all three types of Ca_V2s were eliminated from GCs (Figure 1C; Table S1) (GC [GABRA6], control [CTR] = 15 mice, heterozygote [het] = 24, TKO = 10; GC [α6], CTR = 12, het = 22, TKO = 5). For PCs, deletion of $Ca_V2.1$ led to a high number of paw slips, indicative of a severe motor deficit (Figure 1D; Table S1) (PC [PCP2], CTR = 6 mice, het = 13, TKO = 12). Deletion of $Ca_V2.2$ and/or $Ca_V2.3$ from PCs did not affect motor performance. Together, these results suggest that GC signaling is essential for intact motor performance and that any single Ca_V2 in GCs can support normal motor performance.

Ca_V2 deletion in GCs disrupts synaptic transmission without altering morphology

To interpret the behavioral effects of Ca_V2 deletion, we determined whether there are any gross morphological alterations of the cerebellar cortex. We assessed this using immunohistochemistry to label PCs (Figure 2A, anti-calbindin, green) and targeting a nuclear protein to allow visualization of GCs (Figure 2A, anti-NeuN, red). A sagittal section from a CTR animal (Figure 2A, top left) shows the characteristic lobules and layers of the cerebellar cortex, and an expanded view shows the many GCs of the GC layer, the PC cell bodies of the PC layer, and the PC dendrites within the molecular layer (Figure 2A, bottom left). The cerebellar cortex appeared normal in GC (GABRA6) TKO mice (Figure 2A, center). Although our primary focus was GC TKO mice, we also examined the effects of deleting Cav2.1, Cav2.2, and Cav2.2 in PCs (PC TKO mice) to contrast the effects of the same manipulation of GCs and PCs. In PC TKO mice, the cerebellar cortex was smaller, there were many fewer PCs, and the remaining PCs were diminished in size (Figure 2A, right). PC cell death has also been documented in many mouse models of ataxia,[4–7] and PC 2.1 KO mice also showed a decrease in the number of PCs (Figure S1). We also observed relatively higher numbers of PCs in lobule 10, as reported in other cerebellar neurodegeneration models.[36] In contrast to PC TKO mice, there are no obvious morphological differences in the cerebellum of GC TKO mice.

Another important factor in interpreting behavioral effects in GC TKO mice and PC TKO mice is the extent of the impairment of Cav2.1, Cav2.2, and Cav2.2 signaling. In cultured cells, this TKO approach virtually eliminated synaptic transmission and reduced presynaptic calcium signals by more than 75% by 2 weeks after cre expression,[27] but it may be possible to further reduce calcium channel levels by waiting longer. The onset of cre expression is also important. In PCP2-cre mice, cre is expected to be present in most PCs by post-natal day 8 (P8) and in all PCs by P15.[31] In GABRA6-cre and α6-cre mice, cre is expressed in the majority of GCs by P15[33] and P14,[32] respectively. Last, there is the issue of the fraction of GCs or PCs that express cre. In PCP2-cre mice, cre can drive expression in most PCs.[31] α6-cre mice and GABRA6-cre mice can drive expression in most GCs, but studies with reporter mice leave open the possibility that some GCs will be unaffected.[23,33] However,

it is difficult to extrapolate from reporter studies to calcium channel expression in GCs in our experiments because of differences in genetic loci and differential sensitivity to cre.[37] We considered using immunohistochemistry to quantify calcium channel expression, but it seemed likely that limitations of antibodies and interference from other cell types within the slice would limit our ability to detect and quantify low levels of remaining calcium channels. Ultimately, our goal was to suppress calcium channel expression sufficiently in GCs to strongly perturb synaptic transmission, and the most direct way to address this issue was to quantify transmission at the GC-to-PC synapse.

To assess the extent to which eliminating Ca_V2 disrupts synapse transmission, we performed experiments in brain slices from juvenile and adult mice (Figures 2B and 2C) (juvenile: P31–P36; GC [GABRA6], CTR = 8 cells from 2 mice, TKO = 11 cells from 2 mice; PC [PCP2], CTR = 7 cells from 2 mice, TKO = 7 cells from 2 mice; adult: 7–9 weeks old; GC [GABRA6], CTR = 7 cells from 2 mice, TKO = 8 cells from 2 mice; PC [PCP2], CTR = 4 cells from 2 mice, TKO = 6 cells from 2 mice). We stimulated GC inputs with an extracellular electrode and recorded the resulting excitatory postsynaptic currents (EPSCs) in PCs. EPSCs evoked by single stimuli were strongly reduced in juvenile mice and essentially eliminated in adults (Figure 2B). We also found that synaptic currents evoked by 50-Hz stimulation for 1 s were very strongly attenuated in adult mice (Figure S4). The remaining synaptic transmission in juveniles may reflect incomplete removal of calcium channels in juvenile animals as a consequence of late developmental cre expression that reaches an adult level at P15 in GABRA6-cre mice.[33] The elimination of GC-PC transmission is consistent with the essential contributions of Ca_V2 channels to synaptic transmission and suggests that Ca_V2 channels are eliminated from the vast majority of GCs in GC (GABRA6) TKO mice. These results differ from studies in which Cav2.1 was eliminated from GCs and attenuated GC-PC EPSC remained, which was attributed to transmission from GCs that did not express cre.[23]

These results suggest that disrupting synaptic transmission contributes to behavioral effects arising from Ca_V2 deletion from GCs. Although we only examined the primary targets of GCs, given the central role of CaV2 channels in fast synaptic transmission, it is highly likely that transmission would be strongly attenuated in GC synapses onto all types of target neurons, including those onto molecular layer interneurons that inhibit PCs. We also found that PC-DCN inhibitory postsynaptic currents (IPSCs) were strongly attenuated in juveniles and adults (Figure 2C). A tiny IPSC remained in PC TKO mice that could either be due to incomplete suppression of PC-to-DCN synapses or from stimulation of a type of DCN interneuron that projects to the cerebellar cortex[38] that might have collaterals within the DCN.[39] Synaptic transmission is suppressed to such a great extent that it is unlikely that alterations in PC firing would have any additional influence on PC regulation of DCN firing. In any event, PC-to-DCN synapses are clearly strongly suppressed in PC TKO mice to an extent that leads to profound motor deficits.

Disruption of GC signaling impairs motor performance

To provide insight into the contribution of GCs to normal motor performance, we studied several motor behaviors.[21–23] We focused our behavioral tests primarily on GC TKO mice

because our initial screen indicated that behavioral deficits were only observed reliably in mice in which all Ca_V2 channels had been eliminated from GCs. α6-cre and GABRA6-cre mice have been widely used to target GCs,[23,24,34,40–43] and within the cerebellar cortex, cre is only present in GCs for both cre lines.[32,33] Each of these lines has some off-target cre expression[32,33,43] outside of the cerebellum, but as noted previously,[32] these lines complement each other because they have different patterns of cre expression outside of the cerebellum. In GABR6-cre mice, extracerebellar expression is most prominent in the pontine nucleus,[33,43] whereas in α6-cre mice, a small fraction of neurons scattered within the hippocampus and cortex and a small number of cells in the deep cerebellar nuclei express cre.[32] We therefore performed all behavioral tests in GC (GABRA6) TKO mice and GC (α6) TKO mice and reasoned that off-target contributions, if they exist, would lead to different behavioral deficits when using the two types of cre lines. We also compared behavioral deficits in GC TKO mice and PC TKO mice to determine the relative importance of the input and output layers of the cerebellar cortex.

To determine the influence of GC and PC signaling on balance beam performance, we performed contemporaneous experiments using GC (GABRA 6) TKO mice and PC TKO mice (Figure 3A). We used a breeding strategy that yielded a large fraction of TKO mice (STAR Methods, Mice) rather than using the approach of our initial screen (Figure 1C). Paw slips were rare in littermate CTR mice, but they were common in GC (GABRA6) TKO mice and PC TKO mice (Figure 3A, top) (GC [GABRA6], CTR = 22 mice, TKO = 23; PC [PCP2], CTR = 18, TKO = 15). The traverse time was also significantly increased for GC (GABRA6) TKO mice and PC TKO mice (Figure 3A, bottom). Based on the number of paw slips and the traverse time, the extent of impairment in the balance beam test was comparable for GC (GABRA6) TKO mice and PC TKO mice.

We subsequently assessed balance beam performance in GC (α6) TKO mice (Figure 3B) (CTR = 6 mice, TKO = 9). These experiments were performed by a different investigator in a slightly different manner that influenced traverse times (STAR Methods, Balance beam test). Nonetheless the number of paw slips and the traverse times significantly increased in GC (α6) TKO mice relative to CTRs, providing confirmation of the importance of GC signaling for balance beam performance. The slight differences in experimental conditions compromise our ability to quantitatively compare GC (α6) TKO mice with GC (GABRA6) TKO mice and PC TKO mice. Nonetheless, there were no differences in the number of paw slips in GC (α6) TKO mice, GC (GABRA6) TKO mice, and PC TKO mice.

In addition to using complementary cre lines to target GCs, we addressed the issue of possible off-target effects by specifically targeting GCs using *RC::PFtox* mice that expresses tetanus toxin light chain (TOXIN) under the control of cre and Flpe.[44] A previous study has shown that using *RC::PFtox* in combination with *Math1*-cre and *hßact::Flpe* transgenes to express tetanus toxin broadly in GCs, the DCN, and many other regions leads to ataxia.[44] The virtually ubiquitous expression of Flpe[45] and widespread expression of cre in these mice[46] led to TOXIN expression in many cell types, including cells in the DCN, and prohibited any conclusion regarding the role of GCs in motor performance.[44] However, the observation that these mice were ataxic suggested that this approach could provide insight into the role of GCs in motor performance, provided tetanus toxin expression is

restricted to GCs. We therefore used a series of injections in the cerebellar cortex to express Flpe in cerebellar GCs and to disrupt GC synapses (STAR Methods). Our goal was to disrupt transmission from a sufficiently large population of GCs to increase the likelihood of producing a motor deficit. We had two CTR groups: one that was not injected with the virus and another that was injected with the virus but was cre negative (Figure 3C, each circle indicates a mouse; numbers of samples are shown in Table S2). This latter group provides a CTR for the effects of injections on motor performance.

We performed balance beam tests at weekly intervals, commencing just before injecting the virus. The initial number of paw slips and the traverse times were similar in all three groups (Figure 3C, week 0), and this remained the case for the next 2 weeks (Figure 3C, weeks 1–2), indicating that the surgical operation for virus injection did not impair motor performance. The mouse group expressing tetanus toxin in GCs had a significant increase in the number of paw slips and traverse times from week 3, which increased for the duration of the experiment (Figure 3C, weeks 3–5). For uninjected CTR mice, the number of paw slips remained constant, and there was no increase in the traverse time for the duration of the experiment. For the injected cre-negative CTR group, there was no significant increase in the number of paw slips or the traverse time for the duration of the experiment, although there was a nonsignificant trend to-ward a small increase in the number of paw slips and the traverse time in weeks 4 and 5. These results establish that selective suppression of GC synapses produces strong deficits in the balance beam test that are independent of off-target effects.

We also used balance beam performance to assess the onset of motor deficits with age. The time course of cre expression in PCP2-cre and GC TKO mice[31–33] and the deficits in synaptic transmission we observe by 4 weeks (Figure S5) suggest that motor deficits might be apparent by 4 weeks of age (GC [GABRA6], CTR = 8 mice, TKO = 7; PC [PCP2], CTR = 7, TKO = 7).

The rotarod test is another widely used test to detect impaired baseline motor performance and motor learning.[47–51] Mice are placed on a rotating rod, the speed is increased in stages, and the time taken to fall off is measured. This is repeated for multiple days, and wild-type mice are able to stay on longer on subsequent days as a result of motor learning. Impaired baseline motor performance leads to a decrease in the time mice are able to stay on the on the rotarod on the first day, whereas impaired motor learning is associated with decreased improvement of performance on subsequent days.

Previous studies of mice with altered GC signaling did not observe impaired baseline performance, but the effects on rotarod learning were less consistent. Disrupting GC signaling in a subset of GCs by doxycycline-dependent and GABRA6-cre dependent tetanus toxin expression did not significantly impair rotarod performance on day 1 but reduced the magnitude of learning on subsequent days.[22] Deletion of $Ca_V2.1$ using the α6-cre line to target GCs did not impair performance on the rotarod test.[23] Moreover, increasing GC excitability by GABRA6-cre-dependent deletion of $\delta GABA_A$ receptor subunits did not affect rotarod performance.[43] The lack of an effect of these GC manipulations on baseline

motor performance and the persistence of motor learning in these mice were surprising. One possible explanation is that these manipulations did not completely eliminate GC signaling.

To extend the studies of GC signaling and rotarod performance, we assessed the rotarod performance of GC TKO mice. On day 1, GC (GABRA6) TKO mice and GC (α6) TKO mice spent significantly less time on the rotarod (Figure 4A, day 1) (GC [GABRA6] CTR [n = 11 mice] vs. TKO [n = 10]; GC [α6] TKO CTR [n = 18 mice] vs. TKO [n = 14]), which is consistent with impaired baseline motor performance. The performance of CTR mice on days 2 and 3 showed a significant improvement compared with day 1 (Figures 4A and 4B) (GC [GABRA6] CTR = 11 mice; GC [α6] CTR = 18; Table S2), but the improvement was strongly impaired in GC (GABRA6) TKO mice and GC (α6) TKO mice (group × time interaction, GC [GABRA6] CTR vs. TKO, $p = 0.0076$; GC [α6] CTR vs. TKO, $p < 0.0001$; Table S2), suggesting that motor learning is disrupted in these mice. Similarly, disrupting PC signaling (Figure 4B) impaired baseline properties (PC [PCP2] CTR [n = 18 mice] vs. TKO [n = 11]) and motor learning (group × time interaction, PC [PCP2] CTR vs. TKO, $p < 0.0001$). In the comparisons between GC (GABRA6) TKO, GC (α6) TKO, and PC (PCP2) TKO, we did not observe differences (Table S2). The statistical test to check whether TKO groups show any increase in performance over 3 days shows that there are no increases at all in GC (α6) TKO mice and PC (PCP2) TKO mice (GC [α6] TKO = 14 mice; PC [PCP2] TKO = 11; Table S2) or only a slight increase in GC (GABRA6) TKO mice (n = 10 mice), indicating that learning is almost absent in these mice. We also analyzed the learning pattern over 3 trials within day 1. It shows a similar pattern to what we observed over 3 days but with less significance (Figure S7).

Disrupting GC signaling produces severe gait abnormalities

The cerebellum has been extensively linked to ataxia in humans and in mice, but previous studies found that altering GC signaling did not alter gait to produce ataxia.[21,23,43] We therefore examined gait in GC TKO mice to determine whether a more complete disruption of GC signaling alters gait. We videotaped mice with three different views (Figure 5A, left) and used deep learning to automatically detect the nose, two forelimbs, two hindlimbs, the rear end near the tail base, and the tail tip (Figure 5A, center). For presentation purposes, we inverted the image and marked each body part with circles with different colors (Figure 5A, right).

Plotting body part positions every 5 ms for multiple strides for mice moving at the same speed (0.15 m/s) (Figures 5B–5D) helped to visualize gait abnormalities. Different CTR mice (Figures 5B–5D, left) had qualitatively similar gaits, but the gaits of TKO mice were obviously unlike their CTR counterparts. The clearest differences were that for GC (GABRA6) TKO mice (Figure 5B, right); the tail and the base of the tail had larger deflections than for CTR mice (Figure 5B, left). Similar gait abnormalities were observed in GC (α6) TKO mice (Figure 5C) and PC TKO mice (Figure 5D). A video shows the gaits of the different genotype mice shown in Figure 5 (Video S1).

We quantified gaits in different groups of mice and focused on horizontal and vertical tail position, vertical rear position, and forepaw width (Figure 6A), which were all strongly affected in TKO mice. Experiments were performed with three different types of TKO mice

along with littermate CTR animals. Each parameter was determined for each gait cycle, and the resulting data are presented in three different ways (Figure 6B). First, scatterplots are shown (Figure 6B, columns 1–3), where each point is a parameter plotted as a function of speed for TKO mice (colored) and CTR mice (black) (GC [GABRA6], CTR = 681 cycles from 7 mice, TKO = 789 cycles from 6 mice; GC [α6], CTR = 773 cycles from 6 mice, TKO = 1499 cycles from 9 mice; PC [PCP2], CTR = 534 cycles from 6 mice, TKO = 867 cycles from 6 mice). Some parameters, such as horizontal tail position, were velocity dependent. All of the parameters plotted here are larger in GC (GABRA6) TKO mice, GC (α6) TKO mice, and PC TKO mice. Violin plots for all cycles measured in mice moving at 0.1–0.2 m/s showed statistically significant differences for all parameters for all types of TKO mice (Figure 6B, column 4) (GC [GABRA6], CTR = 393 cycles from 7 mice, TKO = 479 cycles from 6 mice; GC [α6], CTR = 81 cycles from 6 mice, TKO = 429 cycles from 9 mice; PC [PCP2], CTR = 278 cycles from 6 mice, TKO = 444 cycles from 6 mice). Finally, we compared the average parameters for each mouse and found that there were statistically significant differences for each parameter for all TKOs (Figure 6B, column 5). There were no differences in the comparisons between TKOs (Table S2). These comparisons establish that there are gait abnormalities in GC (GABRA6) TKO mice and GC (α6) TKO mice and that these abnormalities are similar to those observed in PC TKO mice.

Disrupting GC signaling impairs locomotion-matched PC firing change

It is difficult to predict how suppressing GC synapses will alter PC firing and the output of the cerebellar cortex. PCs fire spontaneously in the absence of synaptic inputs, tens of thousands of GCs excite each PC to elevate firing, and GCs also activate molecular layer interneurons to disynaptically inhibit PCs. One study found that disrupting GC signaling in a subset of GCs by doxycycline-dependent and GABRA6-cre-dependent tetanus toxin expression eliminated simple spikes in PCs.[21] Another study found that deletion of $Ca_V2.1$ using the α6-cre line did not significantly alter the rate of simple spikes.[23] It is difficult to reconcile these observations.

We measured PC firing in CTR and GC TKO mice to determine how a more complete disruption of GC synapses alters PC firing. We recorded PC firing using a silicon probe in the anterior vermis (lobules 1–4) in awake, head-restrained mice that were free to run on a cylindrical treadmill. We observed typical simple spikes and complex spikes from CTR mice and GC (GABRA6) TKO mice (Figure 7A). The rates of simple spikes and complex spikes were unchanged in GC (GABRA6) TKO mice compared with CTR mice (Figures 7B, left, and 7C). We also analyzed the simple spike coefficient of variance (CV) and CV2, which are measures of the level of simple spike rate variation. CV (Figure 7B, center) and CV2 (Figure 7B, right) were reduced in GC (GABRA6) TKO mice (simple spikes, CTR = 26 cells from 4 mice, TKO = 26 cells from 5 mice; complex spikes, CTR = 9 cells from 2 mice, TKO = 7 cells from 2 mice). These results indicate that disrupting GC signaling does not affect overall PC firing rates but has a small effect on the statistics of PC firing.

Monitoring the self-paced locomotion of the mouse on the treadmill allowed us to determine the influence of locomotion on PC firing. In CTR mice, locomotion was accompanied by an increase in the simple spike rate (Figure 7D, top), whereas in GC (GABRA6) TKO mice, the

simple spike rate did not significantly change during locomotion (Figure 7D). We analyzed PC firing for all transitions from prolonged inactivity to locomotion. Heatmaps of PC firing for onset of locomotion are shown (Figure 7E, left) (CTR = 98 responses from 16 cells, TKO = 29 responses from 13 cells). We observed diverse patterns in firing rate at the onset of locomotion (Figure 7E, left), but approximately half of the events were accompanied by an increase in firing in CTR mice. These firing rate increases did not occur for most events in TKO mice. At the onset of locomotion, the average firing rate increased in CTR mice but not in GC (GABRA6) TKO mice (Figure 7E, top right). For statistical comparison, we calculated the average simple spike rate during locomotion over the inactive period for all cells (Figure 7E, bottom right) (CTR = 16 cells from 4 mice, TKO = 13 cells from 5 mice). In CTR mice, locomotion was accompanied by a significant increase in simple spike rate at the onset of locomotion (one sample t test, $t(15) = 2.53$, $p = 0.023$), but for GC (GABRA6) TKO mice, locomotion did not significantly alter firing (one sample t test, $t(9) = 2.53$, $p = 0.0809$). The firing rate ratios between the CTR and GC (GABRA6) TKO mice were also significantly different (two-tailed t test, $t(24) = 3.14$, $p = 0.0045$). We also analyzed PC firing when locomotion stopped (Figure 7F) (CTR = 78 responses from 17 cells, TKO = 31 responses from 13 cells). There was no significant difference in firing rates for CTR and GC (GABRA6) TKO mice (CTR, one sample t test, $t(16) = 1.56$, $p = 0.139$; TKO, one-sample Wilcoxon test, $W = 29$, $p = 0.1602$), but for CTR mice, simple spike rates tended to decrease slightly. There was a significant difference in the ratio of simple spike rates during the inactive period over the locomotion period for CTR and GC (GABRA6) TKO mice (Figure 7F, bottom right) (CTR = 17 cells from 4 mice, TKO = 13 cells from 5 mice). Together, these results indicate that disruption of GC signaling does not alter spontaneous PC firing, but it prevents locomotion-related increases of PC firing.

DISCUSSION

Our main finding is that GC signaling is essential for normal motor performance. Eliminating expression of all Ca_V2 calcium channels in GCs disrupted synaptic transmission and produced severe deficits in balance beam and rotarod performance and gait. Disrupting GC signaling left PC firing intact *in vivo* and did not increase the CV of firing, but it prevented locomotion-dependent increases in PC firing. These findings suggest that the flow of signals through the cerebellar cortex is required for normal motor performance.

Only strong suppression of GC signaling impairs motor performance

Our finding that disrupting GC signaling profoundly impairs motor performance contrasts with previous studies that also suppressed GC signaling but without robust effects on motor performance. This is likely because we more severely impaired GC signaling. Previously it has been shown that deletion of $Ca_V2.1$ using the α6-cre line to target GCs did not affect performance on the balance beam test or the rotarod test and did not affect gait.[23] GC-to-PC transmission was strongly reduced in these mice, but about 25% of transmission remained. Based on several findings, including the observation that transmission remained sensitive to the selective $Ca_V2.1$ blocker ω-Agatoxin-IVA in these mice, it was concluded that the remaining transmission was primarily a consequence of a functionally intact subset of GCs that did not express cre (14%–25%) in the α6-cre line.Our studies suggest that $Ca_V2.2$

and $Ca_V2.3$ channels present in GCs in their mice may have contributed to the lack of a motor deficit. Another explanation is that the previously observed ω-Aga-IVA-sensitive component of transmission may have been mediated by $Ca_V2.1$ channels that remain in young animals. In GABRA6-cre mice, adult levels of recombination are only attained by P15.[33] While the lifetime of calcium channels in presynaptic boutons is not known, it is possible that it takes several weeks for calcium channels to be eliminated in cre-expressing cells. This is supported by our observation that, in GC (GABRA6) TKO mice, transmission at GC→PC synapses was strongly reduced in juvenile mice but eliminated in adult mice (Figure 2B). We confirm the lack of motor deficits in GC (α6) $Ca_V2.1$ KO mice (Table S1, column 7, second to fourth rows from the bottom), which supports the conclusion that a major disruption of GC transmission does not impair motor performance. We extended this approach and found that elimination of $Ca_V2.1$, $Ca_V2.2$, and $Ca_V2.3$ was required to profoundly disrupt motor performance and that the presence of any one of these channels was sufficient to prevent motor impairment. This is consistent with all of these channels contributing to transmission at GC→PC synapses,[23,25,26] but it is nonetheless surprising in light of the fact that elimination of both $Ca_V2.1$ and $Ca_V2.2$ or $Ca_V2.1$ and $Ca_V2.3$ is expected to have a much larger effect on transmission than elimination of any single type of calcium channel.

It has also been shown that disrupting doxycycline-dependent and GABRA6-cre dependent tetanus toxin expression reduced staying time on a balance beam but did not impair gait.[21,22] In these mice, rotarod performance was not significantly impaired on day 1, but on subsequent days, although learning was apparent in Tet/TeNT-expressing mice, the performance was significantly different from CTR mice. Our results were very different, and we again attribute this to our more complete suppression of transmission. High K^+ evoked glutamate release from cerebellar slices of Tet/TeNT-expressing mice that was approximately 40% of that in CTR mice. This suggests that this genetic strategy does not properly suppress transmission from all GCs, which has been reported in numerous studies of doxycycline-induced gene expression.[22,52,53] Again, the lack of effect on gait and other aspects of motor performance is readily explained by the partial effect on transmission in these mice.

It is important to point out that, in our experiments with *RC::PFtox* mice (Figure 3C), we saw motor deficits even though we did not suppress transmission in all GCs throughout the entire cerebellar cortex (despite our extensive injections). Given that synaptic transmission in GCs is strongly suppressed in triple-transgenic RC::PFtox, Math1-cre, hBact::Flpe mice,[44] it is likely that, in these experiments, we are able to silence the vast majority of GCs in targeted regions. This contrasts with doxycycline-dependent and GABRA6-cre dependent tetanus toxin expression and α6-cre dependent elimination of $Ca_V2.1$, which both leave some GC transmission intact in all regions of the cerebellum. This suggests that profoundly disrupting GC signaling in certain regions of the cerebellar cortex is sufficient to produce motor deficits.

The motor deficits we describe also have important implications for the ability of the cerebellum to compensate for decreases in GC signaling. A previous study of mice with strongly attenuated GC-PC signaling that did not observe a deficit in normal motor

performance suggested that collateral inputs from MFs and/or climbing fibers might be able to compensate for GC loss.[23] Our findings show that, if such a mechanism exists, then it is limited and cannot compensate for complete elimination of GC signaling.

Motor deficits are a result of suppressing GC signaling

It is highly likely that the deficits in GC TKO mice are primarily a consequence of suppressing GC synapses. For the α6-cre and GABRA6-cre lines, GCs are the only cell type affected in the cerebellar cortex. Although both lines express some cre outside of the cerebellar cortex, there is little overlap in their off-target expression. GABRA6-cre leads to extensive recombination in the pontine nucleus and the external cuneate nucleus,[33] whereas α6-cre leads to recombination in a small fraction of cells in the neocortex, hippocampus, pontine nuclei, and DCN.[32] Although both lines also target GCs in the dorsal cochlear nucleus, this auditory region is not implicated in motor deficits. We reasoned that, if off-target cre expression is the cause of behavioral deficits, then the behavioral results may differ between cre lines, which was not the case (Figures 1C, 3A, 3B, 4A, 5B, 5C, and 6B). Experiments in which we targeted the cerebellar cortex specifically provided the most compelling evidence for deficits in GC signaling leading to impaired motor performance (Figure 3C). We restricted expression to the cerebellar cortex with AAV injections, and within the cerebellar cortex, the GABRA6-cre line restricted expression to GCs. CTR experiments in mice lacking cre expression did not exhibit the profound deficits in balance beam performance (Figure 3C).

How cerebellar deficits lead to motor deficits

Our measurements of PC firing in GC TKO mice provide insight into how disruption of GC signaling leads to motor deficits and allow us to discriminate between three mechanisms. First, decreased spontaneous PC inhibition from PC death and/or a decreases in PC firing is thought to contribute to ataxia in many mouse models, including SCA1 mice,[4] SCA2-58Q mice,[18] $ATXN2^{Q127}$ mice,[5] $STIM1^{PKO}$ mice,[54] $PMCA2^{-/-}$mice,[55] and $Ca_V3.1^{-/-}$ mice.[56] We find, however, that the simple spike rate is unchanged, and there is no apparent PC cell death in GC TKO mice (Figures 7B, left, and 2A). Also, we find that PC TKO and GC TKO mice have very similar motor deficits, even though ongoing PC inhibition of DCN neurons is only intact in GC TKO mice. These results suggest that decreased PC signaling cannot account for motor deficits in GC TKO mice. Second, an increase in the irregularity of PC firing (i.e., an increase in CV) occurs in many mouse models of ataxia, and it has been proposed that this contributes to motor deficits.[13–16] In contrast, in GC TKO mice, the CV of PC firing was slightly decreased (Figure 7B, center). Interestingly, PCs in GC $Ca_V2.1$ KO mice showed a similar decrease in CV, but these mice did not have a motor deficit.[23] These results indicate that an increase in the CV of PC firing, or even the observed decrease in the CV of PC firing, does not underlie the motor deficits in GC TKO mice. Finally, a decrease in the influence of MFs on PC firing could contribute to ataxia. We were unable to detect any GC-to-PC synaptic response in GC TKO mice (Figure 2B, bottom), in contrast to previous approaches to suppressing GC signaling. We also found that, during locomotion, the average PC firing rate increased in CTR mice but not in GC TKO mice (Figure 7E). In contrast, optokinetic stimulation increased PC firing in CTR animals, but in $Ca_V2.1$ KO mice, these increases were reduced but not eliminated.[23] These findings suggest that interrupting signal

flow from MFs→GCs→PCs→DCN neurons accounts for the motor deficit in GC TKO mice and is sufficient to account for motor deficits in PC TKO mice (Figure 6B).

The combinatorial elimination of Ca_V2 channels

The genetic strategy we used to examine the behavioral roles of GCs and PCs promises to be generally useful in studies of specific cell types in behavior. The combinatorial elimination of calcium channels used in our initial screen allowed us to quickly determine the essential calcium channels in GC signaling and PC signaling using a simple behavioral screen. The contrast between these two cell types was stark. For the balance beam assay, although $Ca_V2.1$ is the only calcium channel that matters for PCs, $Ca_V2.1$, $Ca_V2.2$, and $Ca_V2.3$ are all required for GCs.This rather surprising finding was readily identified using a behavioral screen that allowed us to focus our subsequent studies on the most interesting genotypes. Importantly, elimination of all Ca_V2 channels seemed to be highly effective at suppressing synaptic transmission, but, based on the GC-to-PC synapse, it is important to wait many weeks after cre expression to ensure elimination of all Ca_V2 channels.

Limitations of the study

Our studies required the use of two cre lines and cerebellum-specific injections to determine the behavioral contributions of cerebellar GCs. This study would have benefitted from a better cre line with fewer off-target effects. It will be informative to extend the approach taken here to address the roles of GCs in social behaviors and in various forms of cerebellum-dependent learning.

STAR★METHODS

RESOURCE AVAILABILITY

Lead contact—Requests for further information, resources, and reagents should be directed to the lead contact, Wade G. Regehr (wade_regehr@hms.harvard.edu).

Materials availability—Mouse mutant alleles are either publicly available or will be shared within the limits of existing material transfer agreements.

Data and code availability—All data are provided in the figures and supplemental figures.

This paper does not report original code.

Any additional information is available from the lead contact upon request.

EXPERIMENTAL MODEL AND SUBJECT DETAILS

Mice—Animal procedures have been carried out in accordance with the NIH and Animal Care and Use committee (IACUC) guidelines, and protocols approved by the Harvard Medical Area Standing Committee on Animals. Male and female mice were used for experiments. Mice were kept on a mixed background (129Sv/SvJ and B6/C57). Mice were

housed under standard conditions in groups of 2–5 animals on a 12 h light-dark cycle with food and water available *ad libitum*.

To generate the mice in Figures 1C and 1D, we utilized the previously described mouse line that has *floxed* alleles for the conditional ablation of $Ca_V2.1$, $Ca_V2.2$, and $Ca_V2.3$. (*floxed* Ca_V2s line).[27] This mouse line was crossed with an appropriate cre line to produce the mice with the genotype cre(+); $Ca_V2.1$(*flox/wt*), $Ca_V2.2$(*flox/wt*), $Ca_V2.3$(*flox/wt*). This mouse line crossed again with *floxed* Ca_V2s line to produce the mice used in the experiments. In order to produce the mice in Figures 2, 3, 4, 5, 6, and 7, the mice with the genotype cre(+); $Ca_V2.1$(*flox/ flox*), $Ca_V2.2$(*flox/ flox*), $Ca_V2.3$(*flox/ flox*) were crossed with the mice with the genotype cre(−); $Ca_V2.1$(*flox/ flox*), $Ca_V2.2$(*flox/ flox*), $Ca_V2.3$(*flox/ flox*). In Figures 5 and 6, 3 mice for the GC (GABRA6) group were generated by crossing cre(+); $Ca_V2.1$(*flox/ flox*), $Ca_V2.2$(*flox/ flox*), $Ca_V2.3$(*flox/ wt*) and cre([−]); $Ca_V2.1$(*flox/ flox*), $Ca_V2.2$(*flox/ flox*), $Ca_V2.3$(*flox/ flox*). In Figure 3C, we crossed *RC::PFtox* mice and GABRA6-cre mice, and the produced mice were again crossed with *RC::PFtox* mice, resulting in *RC::PFtox* allele to be homozygous (*RC::PFtox*(*flox/flox*)) and cre allele to be either heterozygous (GABRA6-cre(+)) or wild type (GABRA6-cre(−)). The GABRA6-cre(−) mice were used as control mice (GABRA6(cre-)-AAV-TOXIN mice).

METHOD DETAILS

Immunohistochemistry and imaging—In Figure 2A, 8–11 week old mice were used. Mice were anesthetized with an intraperitoneal injection of a ketamine (100 mg/kg) and xylazine (10 mg/kg) mixture and perfused with ice cold phosphate buffered saline (PBS, pH = 7.4, Sigma Cat# P-3813), followed by a solution containing 4% paraformaldehyde in PBS. Brains were removed and postfixed in the same solution at 4°C overnight. For slicing, the brain was sliced (50 μm thick) in PBS using a vibratome (VT1000S, Leica). Slices were incubated in a solution containing 0.2% TritonX (Sigma Cat# T9284) and 3% normal goat serum in PBS for 40 minutes. Slices were then incubated in a PBS solution containing primary antibodies (mouse anti-NeuN, 1:500; rabbit anti-Calbindin, 1:1000) overnight at room temperature. Slices were then rinsed 3 times for 10 minutes in PBS. Slices were then incubated in a PBS solution containing secondary antibodies (anti-mouse alexa 568, 1:400; anti-rabbit alexa 647, 1:1000) for 2 hours at room temperature, followed by 3 washes in PBS for 10 minutes. Slices were then mounted on slides (Superfrost Plus, VWR, Cat# 48311-703) and covered with mounting medium (ProLongDiamond, Thermo Fisher Scientific, Cat# P36961) and a glass coverslip. Images were acquired by Axiovision 4 software on a fluorescence microscope Zeiss Axio Imager Z2. Images were processed using standard routines in Fiji (ImageJ).

Slice preparation for electrophysiology—Mice of both sexes were used for physiology experiments. In slice experiments in Figure 2, the postnatal days (P) of the mice used to study the GC to PC synapse were P31–34 (juvenile) and P59–62 (adult). The ages of mice used to study the PC to DCN synapse were P31–36 and P48–49. Animals were anesthetized with ketamine / xylazine / acepromazine and transcardially perfused with warm choline-ACSF solution containing in mM: 110 Choline Cl, 2.5 KCl, 1.25 NaH_2PO_4, 25 $NaHCO_3$, 25 glucose, 0.5 $CaCl_2$, 7 $MgCl_2$, 3.1 Na-Pyruvate, 11.6 Na-Ascorbate, 0.005

NBQX, and 0.0025 (R)-CPP, oxygenated with 95% O2 / 5% CO2. To prepare sagittal slices of the cerebellum, the hindbrain was first removed. A cut was made down the cerebellar midline, and the two halves of the cerebellum were glued with the medial face down to the slicing chamber. 150–200 μm thick sagittal slices were cut with a Leica 1200S vibratome in warm choline-ACSF. Slices were transferred to a standard ACSF solution containing, in mM: 127 NaCl, 2.5 KCl, 1.25 NaH_2PO_4, 25 $NaHCO_3$, 25 glucose, 1.5 $CaCl_2$, and 1 $MgCl_2$ maintained at 34–35°C for 10–12 minutes and then stored at room temperature for at least 20 minutes before beginning recordings.

For GrC to PC synapses, whole-cell recordings were obtained from visually identified granule cells using a 40x water-immersion objective on an upright microscope (Olympus BX51WI). Pipettes were pulled from BF150-86-10 borosilicate glass (Sutter Instrument Co., Novato, CA) at resistances of 4–5 MΩ on a Sutter P-97 horizontal puller. PCs were held at −60 mV. GrC axons were stimulated using a glass monopolar electrode placed in the surrounding white matter. To isolate AMPA glutamatergic currents, the bath included 5 μM SR9553 to block $GABA_A$Rs and 2.5 μM (R)-CPP to block NMDARs.

For PC to DCN synapses, whole-cell voltage clamp recordings were performed on spontaneously active, large diameter (20–25 μm) neurons in the lateral and interposed deep cerebellar nuclei. Large DCN neurons have been characterized as glutamatergic projection neurons.[57] Low resistance (1–2 MΩ) electrodes were used to minimize series resistance (1–8 MΩ), which was compensated up to 80%. Compensation was only applied for the estimated capacitance of the cell body (5 pF). DCN cells were held at −30 to −40 mV. PC axons were stimulated using a glass monopolar electrode placed in the surrounding white matter. To isolate GABAergic currents, the extracellular solution included 5 μM NBQX to block AMPARs, 2.5 μM (R)-CPP to block NMDARs, and 1 μM strychnine to block glycine receptors were included in the bath.

Electrophysiological recordings were performed at~32°C. Borosilicate glass electrodes were filled with a high chloride (E_{Cl} = 0 mV) internal containing in mM: 110 CsCl, 10 HEPES, 10 TEA-Cl, 1 $MgCl_2$, 4 $CaCl_2$, 5 EGTA, 20 Cs-BAPTA, 2 QX314, and 0.2 D600, adjusted to pH 7.3 with CsOH. The flow rate was 5 mL/min. All recordings and analysis were performed blind. Electrophysiology data were acquired using a Multiclamp 700B amplifier (Axon Instruments), digitized at 50 kHz, filtered at 4 kHz, and controlled by software custom written in IGOR Pro (Lake Oswego, OR). Drugs were purchased from Abcam (Cambridge, MA) or Tocris (Bristol, UK). Analysis of electrophysiological data was performed with custom routines written in IgorPro (Wavementrics, Lake Oswego, OR).

Virus injection—Mice (4 weeks) were anesthetized with 2% isoflurane and secured to a stereotaxic frame (Model 940 Small Animal, Kopf Instruments, Tujunga, CA). Eye ointment was applied throughout surgery as needed. The heads of the mice were sanitized with an alcohol-coated wipe and betadine solution. After applying lidocaine, an incision was made to expose the cranium. Then six holes were drilled at the following anterior-posterior (AP) and medial-lateral (ML) coordinates from the bregma: AP:−6.5 and −7.5, ML: 0, −1.9 and +1.9 (mm).Both the GABRA6(cre+)-AAV-TOXIN mice and GABRA6(cre-)-AAV-TOXIN mice were injected by pAAV-EF1a-Flpo (Addgene, 55637-AAV1, titer: 5.0 × 10E12

GC/mL) virus in 6 holes with 3 injections (500 nL/injection) a hole with 0.7, 1.7, and 2.7 mm depths (Nanoject III, Drummond Scientific). The injection rate was less than 3 nL/sec.

Behavioral testing—All motor behavior testing was performed in male and female mice with the experimenter blind to the genotype. For balance beam and rotarod tests, the 8–14 week old mice were used except in Figure 3C where 4 week old mice were used. For gait analysis, 10–15 weeks old mice were used. Before behavioral testing, mice were handled by experimenter for 15 mins for two days. On the test day, mice were transferred to the behavior room and allowed to acclimate for at least 30 min. Apparatuses used for behavioral testing were cleaned with 70% ethanol between experiments.

Balance beam test—Mice were placed at one end of a square beam that was 60 cm long and 1 cm wide and elevated 30 from the bottom. To attract the mice to move, a black box with nesting material inside was placed at the other end of the beam, and an aversive bright lamp (> 600 lux) was installed at the starting side. While the mice move across the beam, the right and left sides of the mice were videotaped by two cameras (ELP, Ailipu Technology Co., 30 Hz frame rate, 640×480 pixel resolution) using iSpy open source software (https://www.ispyconnect.com). Mice were tested until they completed three trials without a two second pause during the trial. Mice were allowed to rest for 1 min between trials. There was a slight difference in the protocol for the GC (α6) group. The black box entrance was covered once the mouse entered the box, whereas it was kept open for GC (GABRA6) and PC (PCP2) groups. For analysis, the number of slips of left and right hindpaws and traverse times were manually counted by the experimenter blind to genotype, and the results of three trials were averaged. Four training trials were performed before the actual trials started, and mice were placed on the beam near the black box (10, 20, 30, 40 cm) to learn to move to the black box. The mice were acclimated in the black box for 5 min prior to training trials.

Rotarod—Mice were placed on a rotating rod device (Rotamex-5 Rota-Rod, Columbus Instruments, Rotamex-5 software). The rod accelerated from 4 rpm to 40 rpm by 1 rpm in 8 s intervals. An animal fall was detected by infrared photo cells crossing the space above the rod and the time-to-fall was automatically recorded. A fall was recorded either if the mouse fell off the rod, or if looped around the rod without running. Mice were tested with 3 trials in a day for three consecutive days. The results of 3 trials were averaged for each day. Animals rested for 1 min between trial.

Gait analysis—Gait analyses were performed as previously described.[43] Mouse gaits were videotaped by a high speed camera (Bonito CL-400B/C, Allied Vision, 2320 × 700 pixel resolution recorded at 200 frames per second) from the bottom side through transparent glass floor while mice walked through a linear corridor illuminated by infrared light. Two mirrors installed on each side allowed simultaneous visualization from below and from both sides. Nesting material was placed at the end of the corridor to attract mice. When the mice reached the end of the corridor, the trial ended, and the recorded video file was saved. Eight trials per mouse per day were recorded for 5 consecutive days.

Videos were analyzed to track the body parts (nose, left and right forepaws, left and right hindpaws, rear-end and tail tip) by using a convolutional neural network as described

previously.[43] Then a hidden Markov model was used to segregate the track into individual gait cycles. The segregated gaits were manually inspected by an experimenter blind to the genotype, and cycles in which body parts were mis-labeled, or during which mice paused or stepped backwards were excluded. We measured the following parameters: cadence, the number of cycles per second; stride length, the maximum distance travelled by a of forepaw within a single cycle; fore- and hindpaw width, the lateral distance between the forepaws or the hindpaws; velocity, the average speed of the center of the mouse (calculated as the distance between the nose and the rear-end along the corridor axis) within a single gait cycle; tail and rear height, the absolute height the tail-tip and rear-end from the floor; tail and rear fluctuation, the standard deviation (SD) of the tail and rear movement (horizontal or vertical). The stride length, paw widths, tail and rear heights and fluctuations were normalized to the body length. For statistics, gait parameters were averaged by cycles and mouse.

***In vivo* recording—**In *in vivo* experiments, recordings were done in GC (GABRA6) TKO mice (11–18 weeks). To prepare for recordings, mice were anesthetized with 2% isoflurane and implanted with a custom-made titanium head bracket. The cranium above the anterior cerebellum remained exposed and was covered with silicone elastomer (Kwik-Sil, World Precision Instruments) at the end of the surgery. Mice were allowed to recover from surgery for at least three days. For acclimation, the mouse was head restrained over a free-moving cylindrical treadmill for at least one session the day before recording. On the day of recording, the mice were anesthetized with 2% isoflurane, and a craniotomy (~0.5mm in diameter) was drilled over the vermis (centered on the midline −6.0 mm posterior to the bregma). After the mouse had been awake for at least an hour, single-unit, multielectrode recordings were made with a silicon probe (E-style 32 channel probes, Cambridge NeuroTech) dipped in Di-I (Vybrant Multicolour Cell Labelling Kit, Thermofisher). *In vivo* recordings from PCs were made while the mouse was awake and head restrained over a freely rotating cylindrical treadmill. Data were sampled at 20 kHz using an RHD2000 recording system (Intan Technologies). Data was filtered between 0.1 and 8kHz. PCs were distinguished by the presence of complex spikes. Treadmill movement was measured using a disassembled optical mouse positioned on the side of the treadmill. Signals were routed to an Arduino which determined the wheel speed. When recordings were complete, mice were perfused with PBS and 4% PFA. 100 μm coronal slices were made from the brain tissue to confirm that the recordings were made in anterior vermis (lobule I - V).

Analysis of *in vivo* electrophysiology—Data were sorted using Plexon Offline Sorter (Plexon Inc, Texas). Analyses were performed using custom MATLAB code (MATLAB R2020b, MathWorks). The coefficient of variation (CV) was calculated by the following formula: standard deviation of interspike intervals (ISI)/(mean of ISI). CV2 was calculated by the following formula: $(2*\text{abs}((ISI_{n+1} - ISI_n))/(ISI_{n+1} + ISI_n))$. Mouse locomotion was monitored by detecting movement of cylindrical treadmill. The definition of ‘locomotion onset’ (Figure 7E) was when the mice started to exhibit 2.5 secs of continuous locomotion preceded by at least 2.5 secs of the inactive state. Similarly, the definition of ‘locomotion end’ (Figure 7F) was when the mice started to show 2.5 secs of an inactive state preceded by at least 2.5 secs of continuous locomotion. In Figure 7E (*right top*), spike rate changes

of each cell were averaged and plotted for +−2.5 secs around the locomotion onset (0.5 sec bin). Similarly, spike rate changes at 'locomotion end' were plotted in Figure 7F (*right top*). In Figure 7E (*right bottom*), the ratio of firing rates during −2.5 to 0 sec and 0 to 2.5 sec was plotted for each cell as a single dot. The ratio values more than 1.0 mean that the firing rate of the cell was increased during 0 to 2.5 sec compared to the firing rate during −2.5 to 0 sec. Similarly, the ratios of firing rates at 'locomotion end' were plotted in Figure 7F (*right bottom*). Among all the recorded data that were used for Figures 7A and 7B, the events of locomotion onsets or locomotion ends were detected, and all the data with the events were plotted in Figures 7E and 7F.

QUANTIFICATION AND STATISTICAL ANALYSIS

Statistical analysis—All statistical tests, significance analyses, number of individual experiments (n) and other relevant information for data comparison are specified in Table S2. Statistical analysis was performed using commercial software (Graphpad Prism 9). For all analyses, normality tests were performed first to appropriately select parametric or non-parametric methods. Significance levels are indicated as *$p < 0.05$, **$p < 0.01$, ***$p < 0.001$ and not significant (ns). No statistical methods were used to predetermine sample sizes. The boxplots were plotted using the MATLAB boxplot function. The bottom and top of each box are the 25th and 75th percentiles of the sample, respectively. The distance between the bottom and top of each box is the interquartile range. The bottom and top error bars indicate the most extreme values within 1.5 times the interquartile range from the 25th and 75th percentiles, respectively.

Supplementary Material

Refer to Web version on PubMed Central for supplementary material.

ACKNOWLEDGMENTS

We thank C. Guo for help with gait analysis experiments. We thank S.M. Dymecki for providing mice. This work was supported by grants from the NIH (R01NS032405 and R35NS097284 to W.G.R.), the Ellen R. and Melvin J. Gordon Center for the Cure and Treatment of Paralysis (to J.-H.L.), and K99NS110978 (to C.H.C.). Imaging was performed in the Neurobiology Imaging Facility at Harvard Medical School.

REFERENCES

1. Hull C, and Regehr WG (2022). The cerebellar cortex. Annu. Rev. Neurosci 45, 151–175. 10.1146/annurev-neuro-091421-125115. [PubMed: 35803588]
2. Shakkottai VG, Chou CH, Oddo S, Sailer CA, Knaus H-G, Gutman GA, Barish ME, LaFerla FM, and Chandy KG (2004). Enhanced neuronal excitability in the absence of neurodegeneration induces cerebellar ataxia. J. Clin. Invest 113, 582–590. 10.1172/JCI20216. [PubMed: 14966567]
3. White JJ, Arancillo M, Stay TL, George-Jones NA, Levy SL, Heck DH, and Sillitoe RV (2014). Cerebellar zonal patterning relies on Purkinje cell neurotransmission. J. Neurosci 34, 8231–8245. 10.1523/JNEUROSCI.0122-14.2014. [PubMed: 24920627]
4. Hourez R, Servais L, Orduz D, Gall D, Millard I, de K. d'Exaerde A, Cheron G, Orr HT, Pandolfo M, and Schiffmann SN (2011). Aminopyridines correct early dysfunction and delay neurodegeneration in a mouse model of spinocerebellar ataxia type 1. J. Neurosci 31, 11795–11807. 10.1523/JNEUROSCI.0905-11.2011. [PubMed: 21849540]

5. Hansen ST, Meera P, Otis TS, and Pulst SM (2013). Changes in Purkinje cell firing and gene expression precede behavioral pathology in a mouse model of SCA2. Hum. Mol. Genet 22, 271–283. 10.1093/hmg/dds427. [PubMed: 23087021]
6. Todorov B, Kros L, Shyti R, Plak P, Haasdijk ED, Raike RS, Frants RR, Hess EJ, Hoebeek FE, De Zeeuw CI, and van den Maagdenberg AMJM (2012). Purkinje cell-specific ablation of CaV2.1 channels is sufficient to cause cerebellar ataxia in mice. Cerebellum 11, 246–258. 10.1007/s12311-011-0302-1. [PubMed: 21870131]
7. Tsai PT, Hull C, Chu Y, Greene-Colozzi E, Sadowski AR, Leech JM, Steinberg J, Crawley JN, Regehr WG, and Sahin M (2012). Autistic-like behaviour and cerebellar dysfunction in Purkinje cell Tsc1 mutant mice. Nature 488, 647–651. 10.1038/nature11310. [PubMed: 22763451]
8. Brown AS, Meera P, Altindag B, Chopra R, Perkins EM, Paul S, Scoles DR, Tarapore E, Magri J, Huang H, et al. (2018). MTSS1/Src family kinase dysregulation underlies multiple inherited ataxias. Proc. Natl. Acad. Sci 115, E12407–E12416. 10.1073/pnas.1816177115. [PubMed: 30530649]
9. Cook AA, Fields E, and Watt AJ (2021). Losing the beat: contribution of Purkinje cell firing dysfunction to disease, and its reversal. Neuroscience 462, 247–261. 10.1016/j.neuroscience.2020.06.008. [PubMed: 32554108]
10. Hoxha E, Balbo I, Miniaci MC, and Tempia F (2018). Purkinje cell signaling deficits in animal models of ataxia. Front. Synaptic Neurosci 10, 6. [PubMed: 29760657]
11. Payne HL, French RL, Guo CC, Nguyen-Vu TB, Manninen T, and Raymond JL (2019). Cerebellar Purkinje cells control eye movements with a rapid rate code that is invariant to spike irregularity. Elife 8, e37102. 10.7554/eLife.37102. [PubMed: 31050648]
12. Hoebeek FE, Stahl JS, van Alphen AM, Schonewille M, Luo C, Rutteman M, van den Maagdenberg AMJM, Molenaar PC, Goossens HHLM, Frens MA, and De Zeeuw CI (2005). Increased noise level of Purkinje cell activities minimizes impact of their modulation during sensorimotor control. Neuron 45, 953–965. 10.1016/j.neuron.2005.02.012. [PubMed: 15797555]
13. Mayoral-Palarz K, Neves-Carvalho A, Duarte-Silva S, Monteiro-Fernandes D, Maciel P, and Khodakhah K (2022). Cerebellar neuronal dysfunction accompanies early motor symptoms in spinocerebellar ataxia type 3. Dis. Model. Mech 15, 049514. 10.1242/dmm.049514.
14. Snell HD, Vitenzon A, Tara E, Chen C, Tindi J, Jordan BA, and Khodakhah K (2022). Mechanism of stress-induced attacks in an episodic neurologic disorder. Sci. Adv 8, eabh2675. 10.1126/sciadv.abh2675.
15. Tara E, Vitenzon A, Hess E, and Khodakhah K (2018). Aberrant cerebellar Purkinje cell activity as the cause of motor attacks in a mouse model of episodic ataxia type 2. Dis. Model. Mech 11, dmm034181. 10.1242/dmm.034181.
16. Walter JT, Alviña K, Womack MD, Chevez C, and Khodakhah K (2006). Decreases in the precision of Purkinje cell pacemaking cause cerebellar dysfunction and ataxia. Nat. Neurosci 9, 389–397. 10.1038/nn1648. [PubMed: 16474392]
17. Jayabal S, Chang HHV, Cullen KE, and Watt AJ (2016). 4-amino-pyridine reverses ataxia and cerebellar firing deficiency in a mouse model of spinocerebellar ataxia type 6. Sci. Rep 6, 29489. 10.1038/srep29489. [PubMed: 27381005]
18. Kasumu AW, Liang X, Egorova P, Vorontsova D, and Bezprozvanny I (2012). Chronic suppression of inositol 1,4,5-triphosphate receptor-mediated calcium signaling in cerebellar Purkinje cells alleviates pathological phenotype in spinocerebellar ataxia 2 mice. J. Neurosci 32, 12786–12796. 10.1523/JNEUROSCI.1643-12.2012. [PubMed: 22973002]
19. Egorova PA, Zakharova OA, Vlasova OL, and Bezprozvanny IB (2016). In vivo analysis of cerebellar Purkinje cell activity in SCA2 transgenic mouse model. J. Neurophysiol 115, 2840–2851. 10.1152/jn.00913.2015. [PubMed: 26984424]
20. Stoyas CA, Bushart DD, Switonski PM, Ward JM, Alaghatta A, Tang MB, Niu C, Wadhwa M, Huang H, Savchenko A, et al. (2020). Nicotinamide pathway-dependent Sirt1 activation restores calcium homeostasis to achieve neuroprotection in spinocerebellar ataxia type 7. Neuron 105, 630–644.e9. 10.1016/j.neuron.2019.11.019. [PubMed: 31859031]
21. Wada N, Kishimoto Y, Watanabe D, Kano M, Hirano T, Funabiki K, and Nakanishi S (2007). Conditioned eyeblink learning is formed and stored without cerebellar granule cell transmission. Proc. Natl. Acad. Sci 104, 16690–16695. 10.1073/pnas.0708165104. [PubMed: 17923666]

22. Yamamoto M, Wada N, Kitabatake Y, Watanabe D, Anzai M, Yokoyama M, Teranishi Y, and Nakanishi S (2003). Reversible suppression of glutamatergic neurotransmission of cerebellar granule cells in vivo by genetically manipulated expression of tetanus neurotoxin light chain. J. Neurosci 23, 6759–6767. 10.1523/JNEUROSCI.23-17-06759.2003. [PubMed: 12890769]
23. Galliano E, Gao Z, Schonewille M, Todorov B, Simons E, Pop AS, D'Angelo E, van den Maagdenberg AMJM, Hoebeek FE, and De Zeeuw CI (2013). Silencing the majority of cerebellar granule cells uncovers their essential role in motor learning and consolidation. Cell Rep 3, 1239–1251. 10.1016/j.celrep.2013.03.023. [PubMed: 23583179]
24. Miyazaki T, Morimoto-Tomita M, Berthoux C, Konno K, Noam Y, Yamasaki T, Verhage M, Castillo PE, Watanabe M, and Tomita S (2021). Excitatory and inhibitory receptors utilize distinct post- and trans-synaptic mechanisms in vivo. Elife 10, e59613. 10.7554/eLife.59613. [PubMed: 34658339]
25. Mintz IM, Sabatini BL, and Regehr WG (1995). Calcium control of transmitter release at a cerebellar synapse. Neuron 15, 675–688. 10.1016/0896-6273(95)90155-8. [PubMed: 7546746]
26. Myoga MH, and Regehr WG (2011). Calcium microdomains near R-type calcium channels control the induction of presynaptic long-term potentiation at parallel fiber to Purkinje cell synapses. J. Neurosci 31, 5235–5243. 10.1523/JNEUROSCI.5252-10.2011. [PubMed: 21471358]
27. Held RG, Liu C, Ma K, Ramsey AM, Tarr TB, De Nola G, Wang SSH, Wang J, van den Maagdenberg AMJM, Schneider T, et al. (2020). Synapse and active zone assembly in the absence of presynaptic Ca2+ channels and Ca2+ entry. Neuron 107, 667–683.e9. 10.1016/j.neuron.2020.05.032. [PubMed: 32616470]
28. Pereverzev A, Mikhna M, Vajna R, Gissel C, Henry M, Weiergräber M, Hescheler J, Smyth N, and Schneider T (2002). Disturbances in glucose-tolerance, insulin-release, and stress-induced hyperglycemia upon disruption of the Cav2.3 (1E) subunit of voltage-gated Ca2+ channels. Mol. Endocrinol 16, 884–895. 10.1210/me.16.4.884. [PubMed: 11923483]
29. Todorov B, van de Ven RCG, Kaja S, Broos LAM, Verbeek SJ, Plomp JJ, Ferrari MD, Frants RR, and van den Maagdenberg AMJM (2006). Conditional inactivation of the Cacna1a gene in transgenic mice. genesis 44, 589–594. 10.1002/dvg.20255. [PubMed: 17146767]
30. Witter L, Rudolph S, Pressler RT, Lahlaf SI, and Regehr WG (2016). Purkinje cell collaterals enable output signals from the cerebellar cortex to feed back to Purkinje cells and interneurons. Neuron 91, 312–319. 10.1016/j.neuron.2016.05.037. [PubMed: 27346533]
31. Zhang X-M, Ng AH-L, Tanner JA, Wu W-T, Copeland NG, Jenkins NA, and Huang J-D (2004). Highly restricted expression of Cre recombinase in cerebellar Purkinje cells. genesis 40, 45–51. 10.1002/gene.20062. [PubMed: 15354293]
32. Aller MI, Jones A, Merlo D, Paterlini M, Meyer AH, Amtmann U, Brickley S, Jolin HE, McKenzie ANJ, Monyer H, et al. (2003). Cerebellar granule cell Cre recombinase expression. genesis 36, 97–103. 10.1002/gene.10204. [PubMed: 12820171]
33. Fünfschilling U, and Reichardt LF (2002). Cre-mediated recombination in rhombic lip derivatives. genesis 33, 160–169. 10.1002/gene.10104. [PubMed: 12203913]
34. Carey MR, Myoga MH, McDaniels KR, Marsicano G, Lutz B, Mackie K, and Regehr WG (2011). Presynaptic CB1 receptors regulate synaptic plasticity at cerebellar parallel fiber synapses. J. Neurophysiol 105, 958–963. 10.1152/jn.00980.2010. [PubMed: 21084685]
35. Luong TN, Carlisle HJ, Southwell A, and Patterson PH (2011). Assessment of motor balance and coordination in mice using the balance beam. J. Vis. Exp 10, 2376. 10.3791/2376.
36. Hernández-Pérez C, Weruaga E, and Díaz D (2023). Lobe X of the cerebellum: a natural neuro-resistant region. Anatomia 2, 43–62. 10.3390/anatomia2010005.
37. Luo L, Ambrozkiewicz MC, Benseler F, Chen C, Dumontier E, Falkner S, Furlanis E, Gomez AM, Hoshina N, Huang W-H, et al. (2020). Optimizing nervous system-specific gene targeting with cre driver lines: prevalence of germline recombination and influencing factors. Neuron 106, 37–65.e5. 10.1016/j.neuron.2020.01.008. [PubMed: 32027825]
38. Ankri L, Husson Z, Pietrajtis K, Proville R, Léna C, Yarom Y, Dieudonné S, and Uusisaari MY (2015). A novel inhibitory nucleo-cortical circuit controls cerebellar Golgi cell activity. Elife 4, e06262. 10.7554/eLife.06262. [PubMed: 25965178]

39. Husson Z, Rousseau CV, Broll I, Zeilhofer HU, and Dieudonné S (2014). Differential GABAergic and glycinergic inputs of inhibitory interneurons and Purkinje cells to principal cells of the cerebellar nuclei. J. Neurosci 34, 9418–9431. 10.1523/JNEUROSCI.0401-14.2014. [PubMed: 25009273]
40. Vinueza Veloz MF, Zhou K, Bosman LWJ, Potters J-W, Negrello M, Seepers RM, Strydis C, Koekkoek SKE, and De Zeeuw CI (2015). Cerebellar control of gait and interlimb coordination. Brain Struct. Funct 220, 3513–3536. 10.1007/s00429-014-0870-1. [PubMed: 25139623]
41. Zhou H, Lin Z, Voges K, Ju C, Gao Z, Bosman LWJ, Ruigrok TJH, Hoebeek FE, De Zeeuw CI, and Schonewille M (2014). Cerebellar modules operate at different frequencies. Elife 3, e02536. 10.7554/eLife.02536. [PubMed: 24843004]
42. Seja P, Schonewille M, Spitzmaul G, Badura A, Klein I, Rudhard Y, Wisden W, Hübner CA, De Zeeuw CI, and Jentsch TJ (2012). Raising cytosolic Cl− in cerebellar granule cells affects their excitability and vestibulo-ocular learning. EMBO J 31, 1217–1230. 10.1038/emboj.2011.488. [PubMed: 22252133]
43. Rudolph S, Guo C, Pashkovski SL, Osorno T, Gillis WF, Krauss JM, Nyitrai H, Flaquer I, El-Rifai M, Datta SR, and Regehr WG (2020). Cerebellum-specific deletion of the GABAA receptor δ subunit leads to sex-specific disruption of behavior. Cell Rep 33, 108338. 10.1016/j.celrep.2020.108338. [PubMed: 33147470]
44. Kim JC, Cook MN, Carey MR, Shen C, Regehr WG, and Dymecki SM (2009). Linking genetically defined neurons to behavior through a broadly applicable silencing allele. Neuron 63, 305–315. 10.1016/j.neuron.2009.07.010. [PubMed: 19679071]
45. Rodríguez CI, Buchholz F, Galloway J, Sequerra R, Kasper J, Ayala R, Stewart AF, and Dymecki SM (2000). High-efficiency deleter mice show that FLPe is an alternative to Cre-loxP. Nat. Genet 25, 139–140. 10.1038/75973. [PubMed: 10835623]
46. Matei V, Pauley S, Kaing S, Rowitch D, Beisel K.w., Morris K, Feng F, Jones K, Lee J, and Fritzsch B (2005). Smaller inner ear sensory epithelia in Neurog1 null mice are related to earlier hair cell cycle exit. Dev. Dyn 234, 633–650. 10.1002/dvdy.20551. [PubMed: 16145671]
47. Jones BJ, and Roberts DJ (1968). The quantitative measurement of motor inco-ordination in naive mice using an accelerating rotarod. J. Pharm. Pharmacol 20, 302–304. 10.1111/j.2042-7158.1968.tb09743.x. [PubMed: 4384609]
48. Hamm RJ, Pike BR, O'dell DM, Lyeth BG, and Jenkins LW (1994). The rotarod test: an evaluation of its effectiveness in assessing motor deficits following traumatic brain injury. J. Neurotrauma 11, 187–196. 10.1089/neu.1994.11.187. [PubMed: 7932797]
49. Buitrago MM, Schulz JB, Dichgans J, and Luft AR (2004). Short and long-term motor skill learning in an accelerated rotarod training paradigm. Neurobiol. Learn. Mem 81, 211–216. 10.1016/j.nlm.2004.01.001. [PubMed: 15082022]
50. Monville C, Torres EM, and Dunnett SB (2006). Comparison of incremental and accelerating protocols of the rotarod test for the assessment of motor deficits in the 6-OHDA model. J. Neurosci. Methods 158, 219–223. 10.1016/j.jneumeth.2006.06.001. [PubMed: 16837051]
51. Shiotsuki H, Yoshimi K, Shimo Y, Funayama M, Takamatsu Y, Ikeda K, Takahashi R, Kitazawa S, and Hattori N (2010). A rotarod test for evaluation of motor skill learning. J. Neurosci. Methods 189, 180–185. 10.1016/j.jneumeth.2010.03.026. [PubMed: 20359499]
52. Das AT, Tenenbaum L, and Berkhout B (2016). Tet-on systems for doxycycline-inducible gene expression. Curr. Gene Ther 16, 156–167. 10.2174/1566523216666160524144041. [PubMed: 27216914]
53. De Boeck J, and Verfaillie C (2021). Doxycycline inducible overexpression systems: how to induce your gene of interest without inducing misinterpretations. Mol. Biol. Cell 32, 1517–1522. 10.1091/mbc.E21-04-0177. [PubMed: 34383558]
54. Ryu C, Jang DC, Jung D, Kim YG, Shim HG, Ryu H-H, Lee Y-S, Linden DJ, Worley PF, and Kim SJ (2017). STIM1 regulates somatic Ca2+ signals and intrinsic firing properties of cerebellar Purkinje neurons. J. Neurosci 37, 8876–8894. 10.1523/JNEUROSCI.3973-16.2017. [PubMed: 28821659]
55. Empson RM, Turner PR, Nagaraja RY, Beesley PW, and Knöpfel T (2010). Reduced expression of the Ca2+ transporter protein PMCA2 slows Ca2+ dynamics in mouse cerebellar Purkinje

neurones and alters the precision of motor coordination. J. Physiol 588, 907–922. 10.1113/jphysiol.2009.182196. [PubMed: 20083513]

56. Ly R, Bouvier G, Schonewille M, Arabo A, Rondi-Reig L, Léna C, Casado M, De Zeeuw CI, and Feltz A (2013). T-type channel blockade impairs long-term potentiation at the parallel fiber–Purkinje cell synapse and cerebellar learning. Proc. Natl. Acad. Sci 110, 20302–20307. 10.1073/pnas.1311686110. [PubMed: 24277825]
57. Uusisaari M, Obata K, and Knöpfel T (2007). Morphological and electrophysiological properties of GABAergic and non-GABAergic cells in the deep cerebellar nuclei. J. Neurophysiol 97, 901–911. 10.1152/jn.00974.2006. [PubMed: 17093116]

Highlights

- Transgenic and viral disruption of granule cell signaling impairs motor performance
- CaV2.1, CaV2.2, and CaV2.3 must all be deleted from GCs to impair motor performance
- Disrupting GC signaling does not alter cerebellar ultrastructure or PC firing rates
- Locomotion-dependent increases in Purkinje cell firing require GC signaling

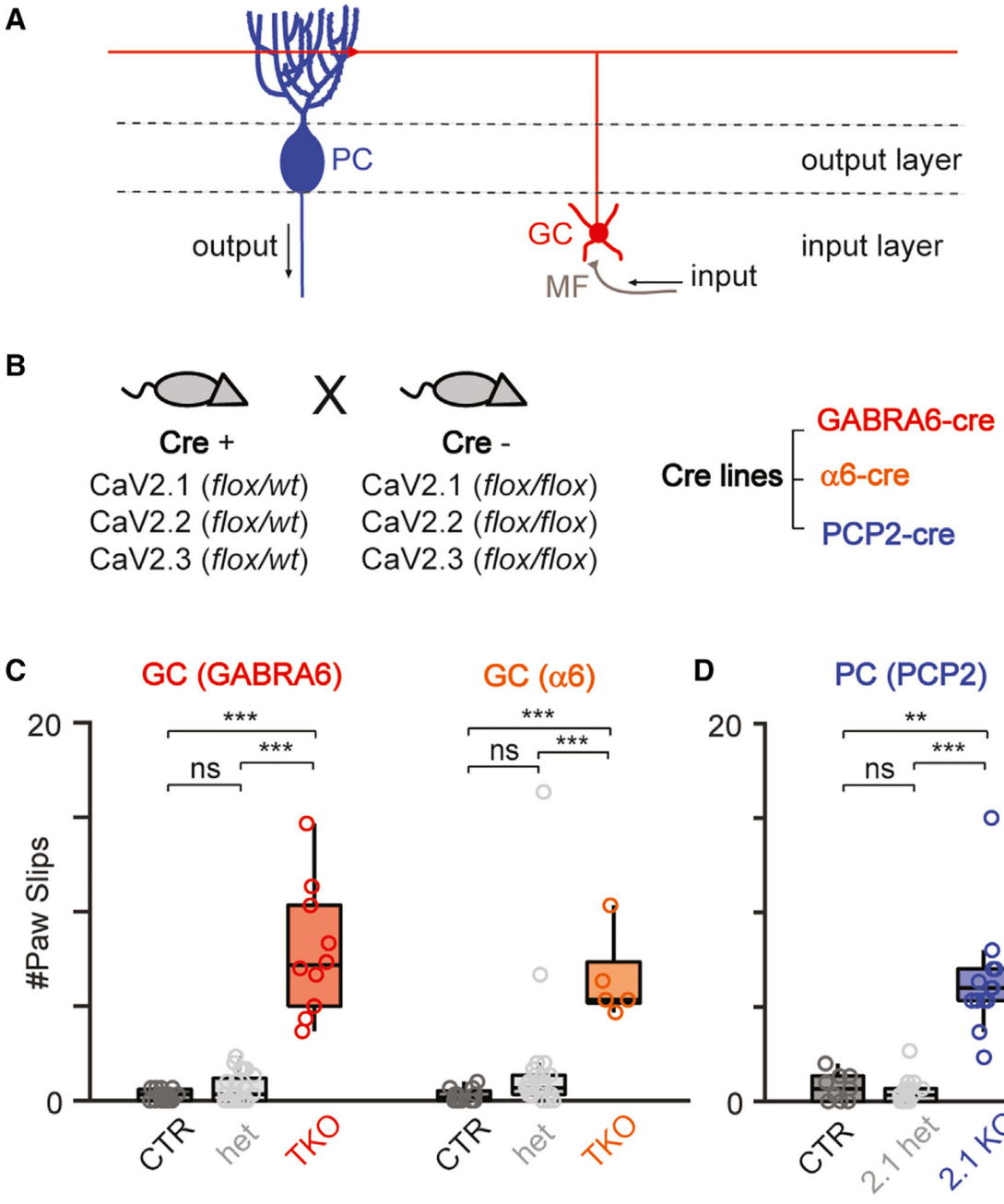

Figure 1. Motor effects arising from elimination of Ca_V2 calcium channels in PCs and GCs

(A) Simplified schematic of the cerebellar cortex. PC, Purkinje cell; GC, granule cell; MF, mossy fiber.

(B) Breeding strategy used to delete different combinations of $Ca_V2.1$, $Ca_V2.2$, and $Ca_V2.3$ calcium channels in GCs or PCs. GABRA6-cre or α6-cre targeted GCs, and PCP2-cre targeted PCs.

(C) Slips for GC TKO mice. Each circle indicates a mouse. A high number of paw slips occurred only when all three Ca_V2s were knocked out (het, heterozygote). See Table S1, column 9, for mouse genotypes.

Mice in (C) and (D) were adults (8–11 week).

(D) Slips for PC (PCP2) mice. A high number of paw slips occurred when $Ca_V2.1$ was knocked out (2.1 KO), regardless of whether $Ca_V2.2$ and/or $Ca_V2.3$ were present. See Table S1, column 12, for mouse genotypes.

**p < 0.01, ***p < 0.001; ns, not significant (Table S2). Boxplots were plotted using MATLAB (STAR Methods, Statistical analysis).

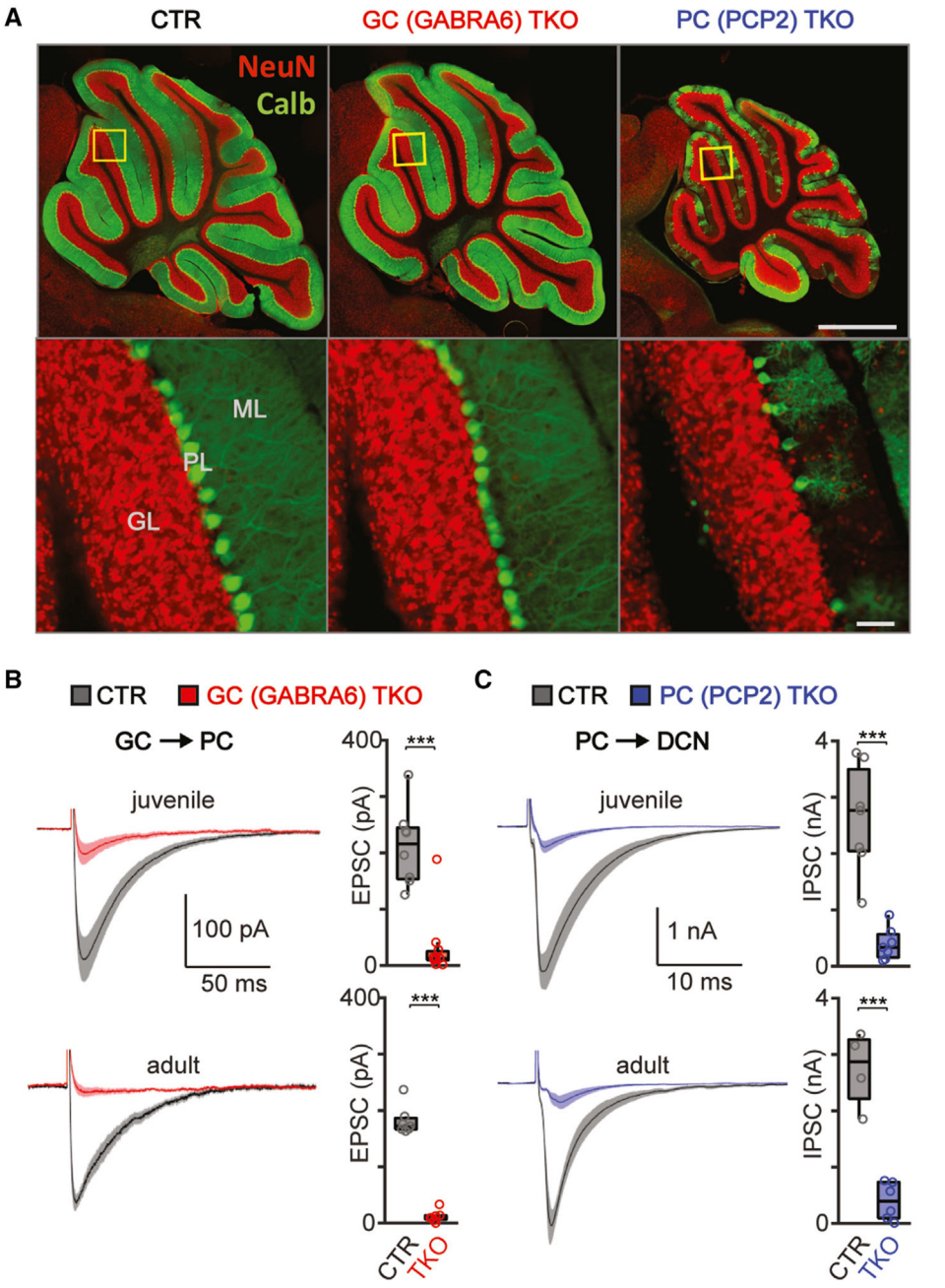

Figure 2. The properties of PC (PCP2) TKO mice and GC (GABRA6) TKO mice

(A) Sagittal sections of the cerebellar cortex in CTR, GC (GABRA6) TKO, and PC (PCP2) TKO mice. Immunostaining against calbindin (Calb; green) labeled PCs and against NeuN (red) labeled nuclei to show the extent of the granular layer (GL) (ML, molecular layer; PL, PC layer). Scale bars, 1,000 μm (top) and 50 μm(bottom). Mice were 11 week old for CTR and GC (GABRA6) TKO and 8 weeks for PC (PCP2) TKO. See also Figures S2 and S3.

(B) GC-PC EPSCs were studied in brain slices using whole-cell recordings. Average GC-PC EPSCs in CTR mice (gray) and in GC (GABRA6) TKO mice (red) are shown (left), and

individual cells are summarized (right). Shadow plots (left) show the mean (line) and SEM (shaded).

(C) PC-DCN neuron synapses were studied in brain slices. Average IPSCs for CTR mice (gray) and PC (PCP2) TKO mice (blue) are shown (left). Individual cells are summarized (right). In (B) and (C), results are shown for juvenile (top, P31–P36) and adult (bottom, 7–9 weeks) mice. ***$p < 0.001$ (Table S2). Boxplots were plotted using MATLAB (STAR Methods, Statistical analysis).

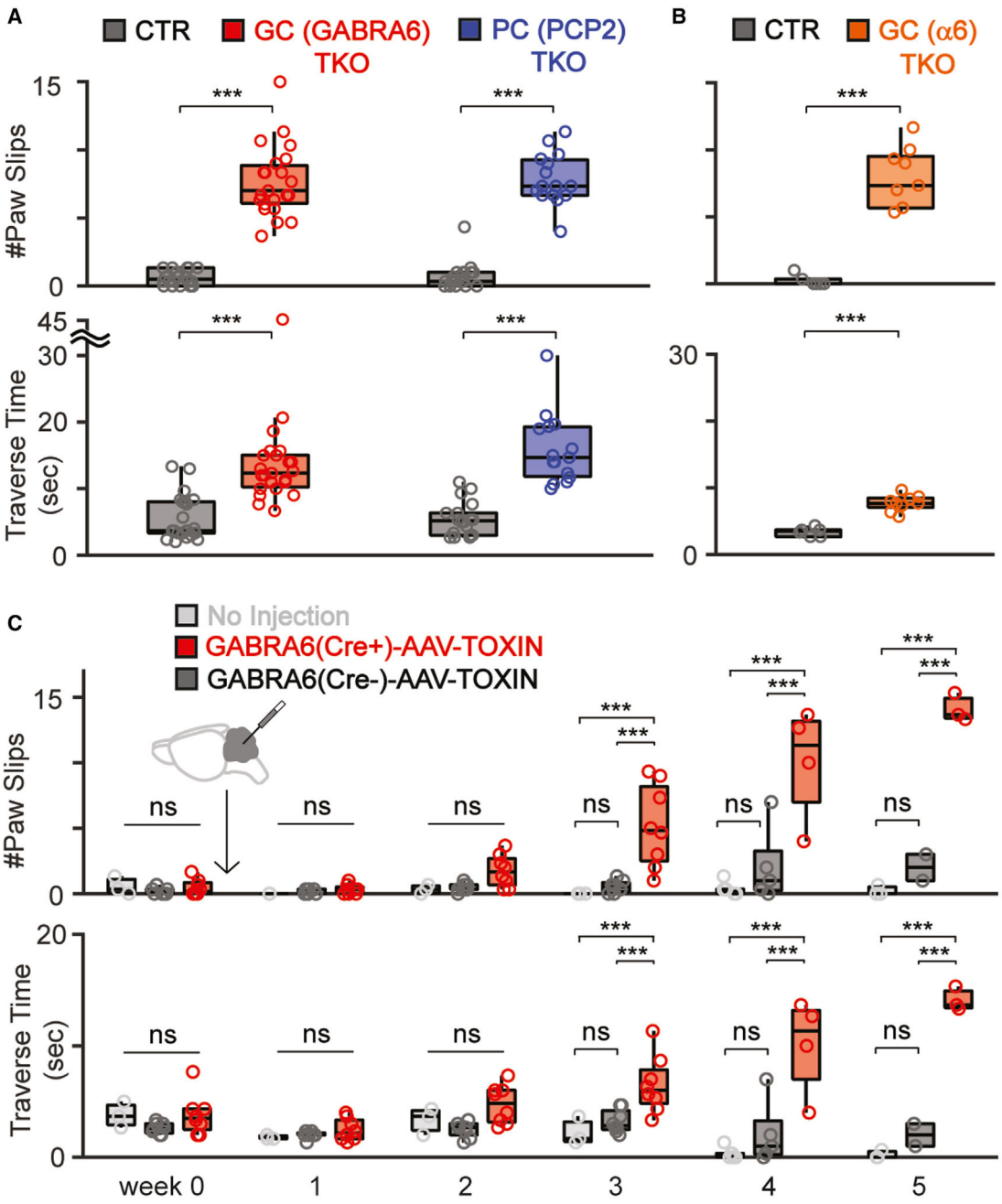

Figure 3. Suppressing GC signaling impairs motor performance

(A and B) The results of the balance beam test. Each circle indicates a mouse. The number of paw slips (top) and traverse time (bottom) are shown for CTR mice (CTR), GC (GABRA6) TKO mice, PC (PCP2) TKO mice, and GC (α6) TKO mice. Mice shown are adults (8–14 weeks). See also Figure S5.

(C) AAV was injected into the cerebellar cortex, and the balance beam test was performed each week for 6 weeks beginning immediately prior to the injection. In one group, there were no injections; in another group, AAV injections were used to selectively suppress GC synapses by expressing tetanus toxin in GCs (GABRA6(cre+)-AAV-Toxin); and in a CTR

group, injections were performed in mice lacking cre (GABRA6(cre-)-AAV-Toxin). Each circle indicates a mouse. Injections were made in 4-week-old mice. See also Figure S6. ***$p < 0.001$ (Table S2). Boxplots were plotted using MATLAB (STAR Methods, Statistical analysis).

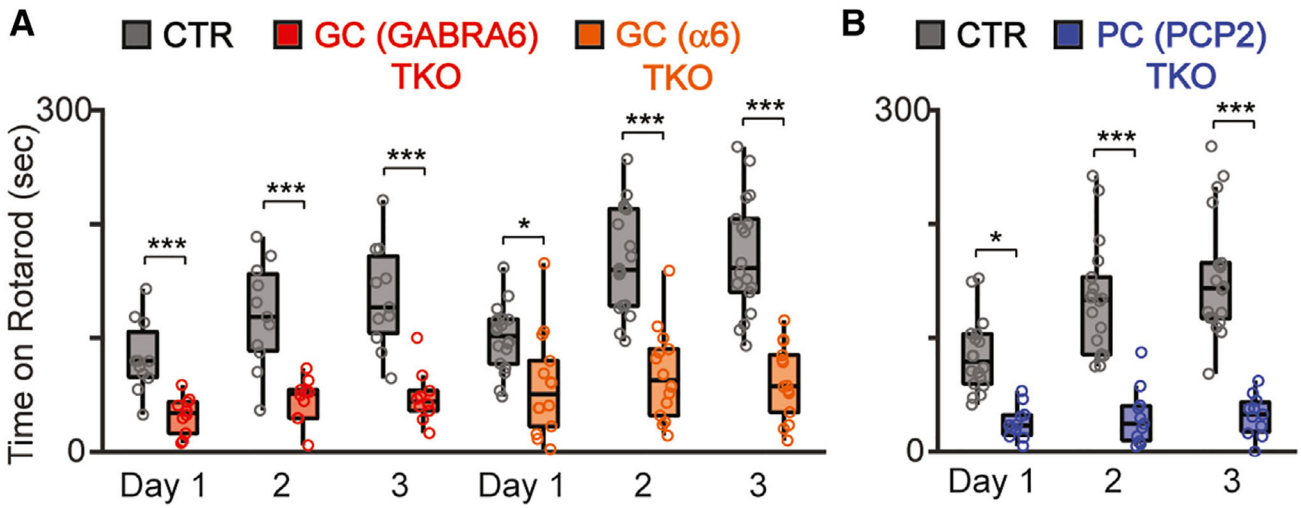

Figure 4. Suppressing GC signaling impairs motor performance and motor learning

(A and B) The results of the rotarod test. Times on the rotarod until mice fell off are shown for GC (GABRA6) TKO, GC (α6) TKOs, and PC (PCP2) TKO mice. Each circle indicates a mouse. All TKO groups showed less time on the rotarod than the CTR groups on all days. CTR groups showed improved performance on successive days, but the improvement was strongly impaired in all TKO groups. Mice were adults (8–14 weeks).

*$p < 0.05$, ***$p < 0.001$ (Table S2). The boxplots were plotted using MATLAB (STAR Methods, Statistical analysis).

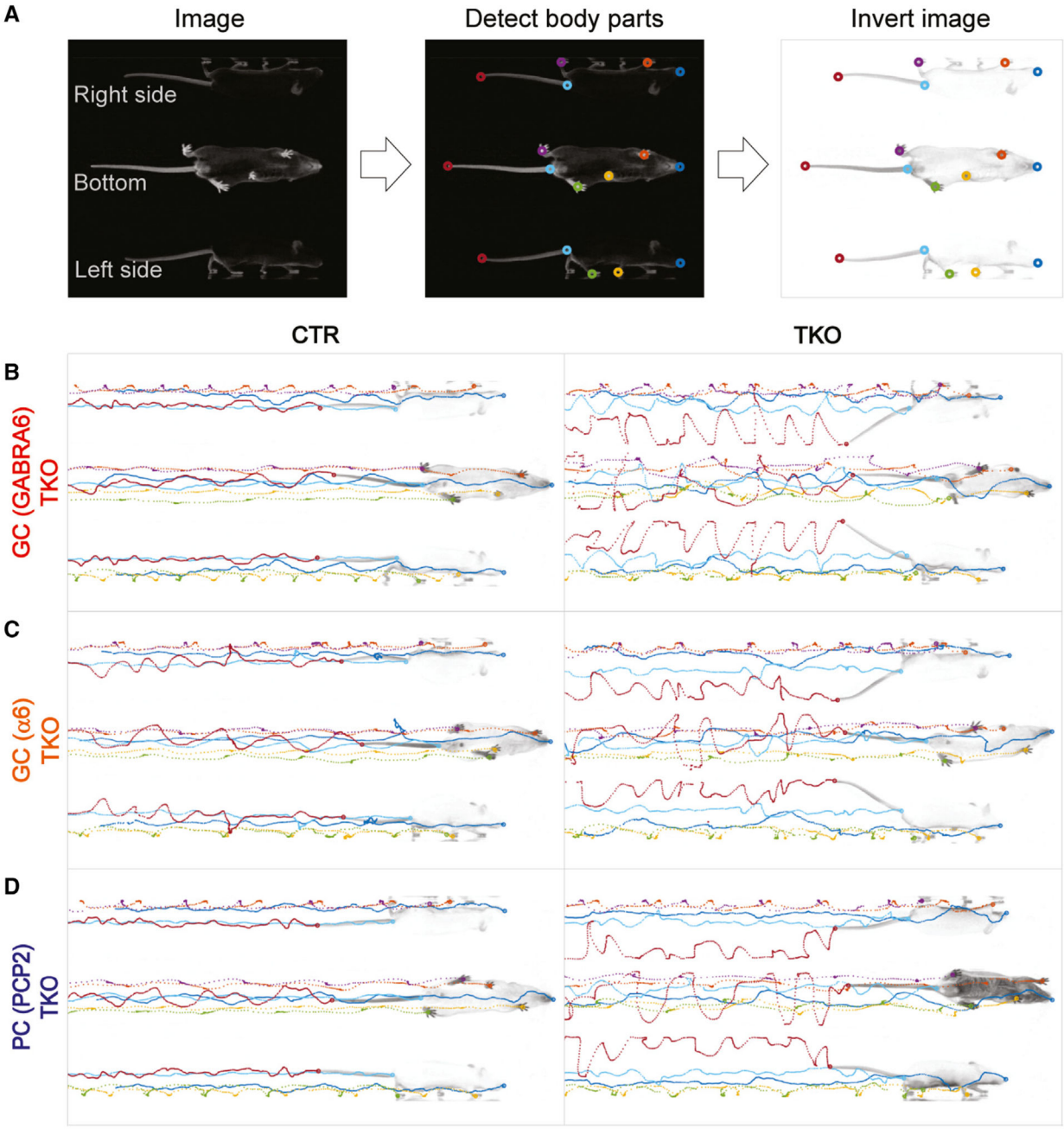

Figure 5. Gait analysis of GC TKO mice and PC TKO mice

(A) Schematic of gait analysis using high-speed video recordings of mice traversing a platform with two side views and a bottom view (left). Multiple body parts were tracked, including the nose, two front paws, two hindpaws, the rear near the base of the tail, and the tail tip (center). The images were inverted for display purposes (right).

(B–D) Traces of body parts during walking at the same speed (0.15 m/s) for CTR mice (left) and TKO mice (right). Each dot is separated by 5 ms

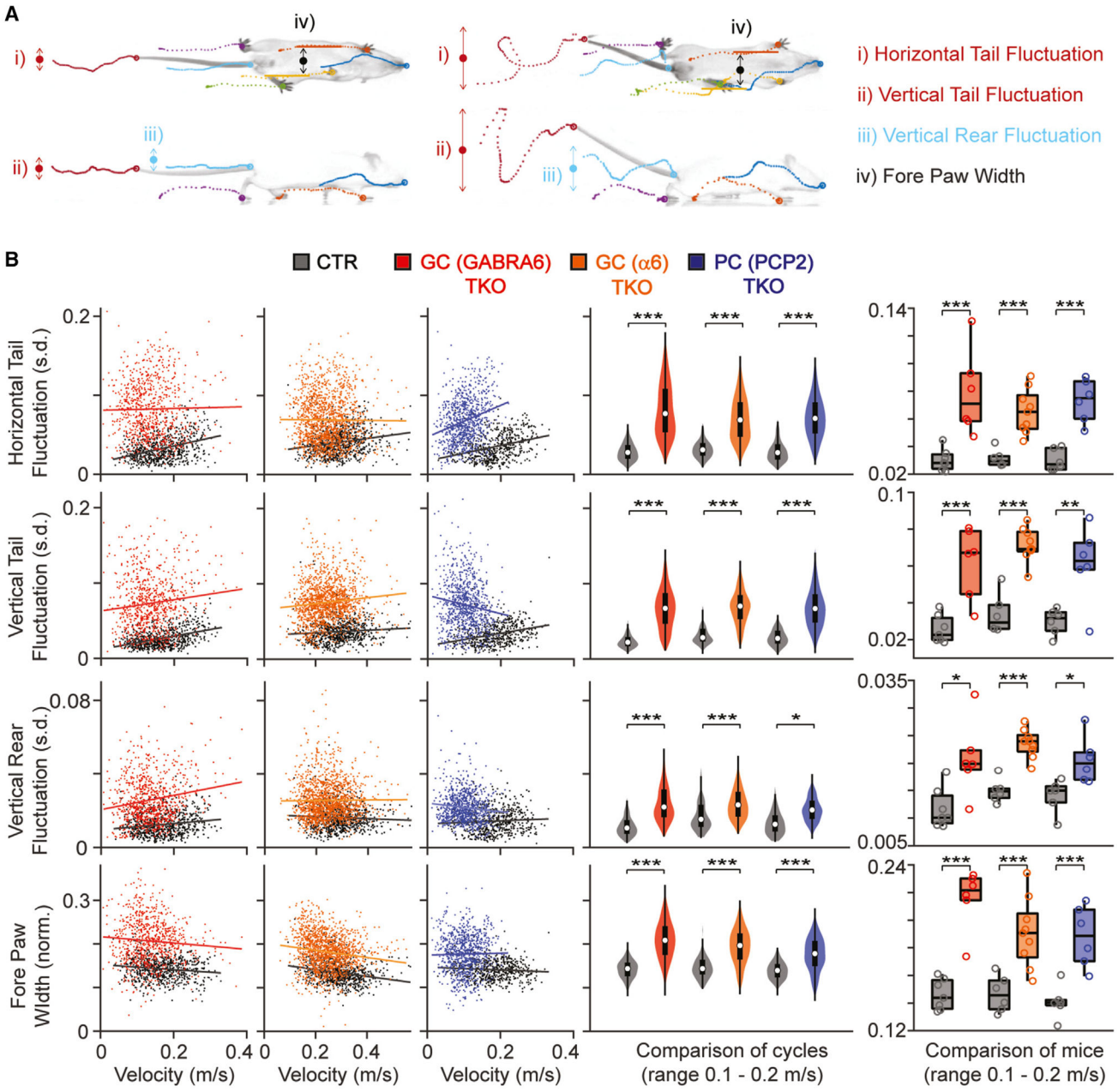

Figure 6. Suppressing GC signaling impairs gait

(A) Traces during a single gait cycle with a bottomand a side view for a CTR (left) and a GC (GABRA6) TKO (right) mouse. Analyzed parameters (i–iv) are indicated.

(B) Different parameters (rows 1–4) are summarized. Each parameter is shown as a function of velocity (columns 1–3), with each dot corresponding to a single cycle and each plot containing regression lines for all points for CTR (black) and TKO mice. Cycles within the velocity range of 0.1–0.2 m/s were compared (column 4). Columns 1–4 are summaries for all cycles for all mice of the indicated genotype. Average results for each mouse were also plotted (column 5; each dot is a mouse). Mice were adults (10–15 weeks).

*p < 0.05, **p < 0.01, ***p < 0.001 (Table S2). Boxplots were plotted using MATLAB (STAR Methods, Statistical analysis).

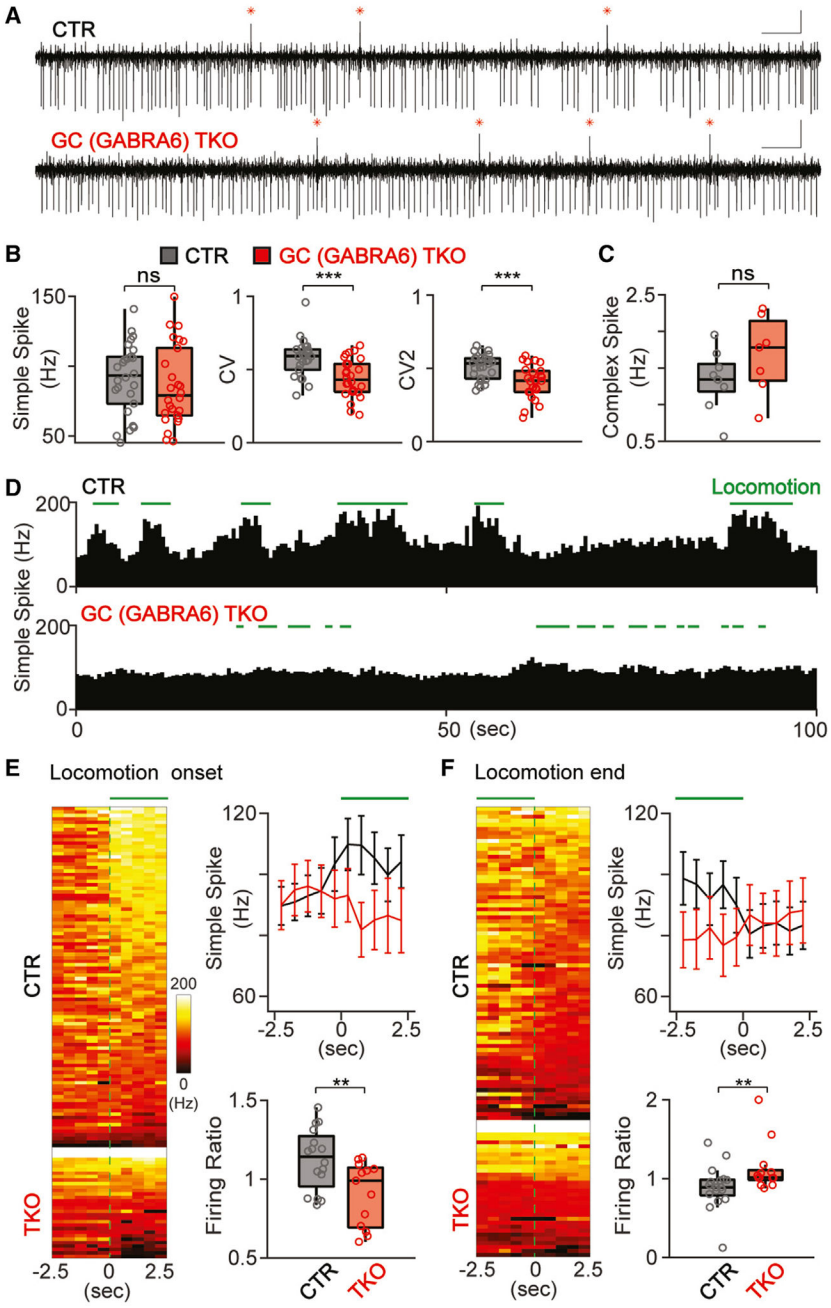

Figure 7. The in vivo PC firing properties in GC (GABRA6) TKO mice

(A) PC firing in a CTR mouse (top) and in a GC (GABARA6) TKO mouse (bottom). Simple spikes and complex spikes (red asterisks) are present. Scale bars, 0.1 s and 0.5 mV.

(B) Simple spike properties are summarized. Each circle indicates a cell.

(C) Complex spike firing rates are summarized. Each circle indicates a cell.

(D) Examples of simple spike firing rates during periods of locomotion (green lines) and inactivity.

(E) Summaries of simple spike firing rates at the onset of locomotion. Heatmaps of firing rates for each onset event (left; each row indicates a single cell response at individual onset

event), the average simple spike firing rate of all recorded PCs (top right, ±SEM), and the ratio of firing rates for 2.5 s before and after locomotion onset (bottom right; each circle indicates a cell) are shown.

(F) Summaries of simple spike firing rates as in (E) but for events in which locomotion stopped.

Mice in (A)–(F) are adults (11–18 weeks). **$p < 0.01$, ***$p < 0.001$ (Table S2). Boxplots were plotted using MATLAB (STAR Methods, Statistical analysis).

KEY RESOURCES TABLE

REAGENT or RESOURCE	SOURCE	IDENTIFIER
Antibodies		
mouse anti-NeuN	Abcam	Cat# ab104224; RRID:AB_10711040
rabbit anti-Calbindin	Abcam	Cat# ab108404; RRID:AB_10861236
anti-mouse Alexa 568	Abcam	Cat# ab175473; RRID:AB_2895153
anti-rabbit Alexa 647	Thermo scientific	Cat# A32733; RRID:AB_2633282
Bacterial and virus strains		
pAAV-EF1a-Flpo (AAV1)	Addgene	Cat# 55637-AAV1; RRID:Addgene_55637
Experimental models: Organisms/strains		
GABRA6-cre mice (B6; D2-Tg(Gabra6-cre)B1Lfr/Mmucd)	MMRRC	RRID: MMRRC_000196-UCD
α6-cre mice (B6; 129P2-Gabra6tm2(cre)Wwis/Mmucd)	MMRRC	RRID:MMRRC_000213-UCD
Pcp2-cre mice (B6.Cg-Tg(Pcp2-cre)3555Jdhu/J)	Jackson laboratory	Strain# 010536; RRID:IMSR_JAX:010536
Mouse: Cacna1a conditional knockout	Todorov et al.[29]	N/A
Mouse: Cacna1b conditional knockout, Cacna1b$^{tm1a(KOMP)Wtsi}$	Held et al.[27]	Cat# KOMP: CSD34514; RRID: IMSR_KOMP: CSD34514-1a-Wtsi
Mouse: Cacna1e conditional knockout	Pereverzev et al.[28]	N/A
Software and algorithms		
Igor Pro 6	Wavemetrics	https://www.wavemetrics.com
MATLAB (R2020b)	MathWorks	https://www.mathworks.com/
Prism 9	Graphpad	https://www.graphpad.com/
Adobe Illustrator	Adobe	https://www.adobe.com/products/illustrator.html
Plexon Offline Sorter 3	Plexon	https://plexon.com